

**3D PRINTING OF BIOCOMPATIBLE CRYOGELS FOR  
BONE TISSUE ENGINEERING**

**Muhammad Moazzam, MPhil Public Health**

**Submitted in fulfillment of the requirements for the degree of  
Master of Science in Biomedical Engineering**



**School of Engineering and Digital Sciences  
Department of Chemical & Materials Engineering  
Nazarbayev University**

53 Kabanbay Batyr Avenue,  
Astana, Kazakhstan, 010000

**Supervisor:** Prof. Dana Akilbekova

**Co-Supervisor:** Prof. Nurxat Nuraje

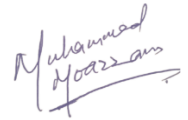
# Dedication

*To my mother and in memory of my grandma  
For their love and kindness throughout my life*

# Declaration

I hereby, declare that this manuscript, entitled “3D PRINTING OF BIOCOMPATIBLE CRYOGELS FOR BONE TISSUE ENGINEERING ”, is the result of my own work except for quotations and citations which have been duly acknowledged.

I attest that, as far as I am aware, the work has not been presented, in part or in its entirety, for any other academic degree or diploma at Nazarbayev University or any other institution, either nationally or internationally.



---

Name: Muhammad Moazzam  
Date: 02-05-23

# ABSTRACT

Natural biopolymers are highly valued and commonly utilized in tissue engineering to create scaffolds that support living cells. This is due to their exceptional biocompatibility and the fact that their degradation rate can be controlled. However, the shape and average pore size are crucial in biological processes that influence the kinetics of cell proliferation and tissue regeneration processes linked to the production of extracellular matrix. For the construction of high-accuracy hydrogel scaffolds via 3D printing, the shear thinning characteristics of the bioinks used frequently result in morphological compromises like smaller pore diameters. Here, we introduced a new mixture of gelatin and oxidized alginate (Gel/OxAlg) that has been optimized for use in 3D printing and cryogelation techniques. This composite formulation allows for the creation of highly porous and biocompatible hydrogel scaffolds with extra-large pore sizes ( $d > 100 \mu\text{m}$ ) using a combination of 3D printing and cryogelation techniques. These scaffolds have the potential to serve as a platform for various tissue engineering applications, and their morphological properties and cell viability data can be tailored accordingly. Overall, our approach offers a simple and cost-effective method for constructing hydrogel scaffolds with high accuracy.

# Acknowledgments

First and foremost, I'd want to thank my supervisors, Prof. Dana Akilbekova and Dr. Alexander Trifonov, for their guidance and help, as well as for the opportunity to work under their supervision. Second, I am appreciative of the in vivo experiment coordination of group members Dana Sultanova and Fariza Mukasheva, as well as occasional assistance from Ahmer Shahzad and Birzhan Abdikhan.

# Table of Content

<b>Dedication</b> .....	<b>2</b>
<b>Declaration Form</b> .....	<b>3</b>
<b>ABSTRACT</b> .....	<b>4</b>
<b>Acknowledgments</b> .....	<b>5</b>
<b>List of abbreviations</b> .....	<b>8</b>
<b>List of Figures</b> .....	<b>9</b>
<b>Chapter 1- INTRODUCTION</b> .....	<b>11</b>
<b>1.1. Human Bone:</b> .....	<b>11</b>
<b>1.1.1. The function of bone in the body:</b> .....	<b>11</b>
<b>1.1.2. Bone development process:</b> .....	<b>11</b>
1.1.2.1. Osteoblasts:.....	12
1.1.2.2. Osteocytes: .....	12
1.1.2.3. Osteoclasts:.....	13
<b>1.1.3. Bone structure and composition:</b> .....	<b>13</b>
<b>1.2. Bone Tissue Engineering (BTE):</b> .....	<b>14</b>
1.2.1. Scaffolds in Bone Tissue Engineering (BTE):.....	16
1.2.2. Biomaterials used for Scaffolds Fabrication: .....	16
1.2.3. Crosslinking in the 3D Printed Scaffolds:.....	18
1.2.4. Morphology of scaffoldsand its effect on tissue development: .....	19
1.2.5. Cryogelation: .....	21
1.2.6. Stability and integrity of scaffold: .....	21
1.2.7. Scaffold fabrication techniques: .....	22
1.2.8. 3D bioprinting in bone tissue engineering: .....	24
<b>1.3. Thesis statement:</b> .....	<b>26</b>
<b>1.4. Aims and Objectives:</b> .....	<b>26</b>
1.4.1. Aim:.....	26
1.4.2. Objectives:.....	26
<b>CHAPTER 2. METHODS AND MATERIALS</b> .....	<b>27</b>
<b>2.1. Chemicals:</b> .....	<b>27</b>

<b>2.2. Synthesis of biopolymer and formulation of ink:</b>	27
<b>2.3. Shear thinning properties:</b>	27
<b>2.4. 3D printing of Scaffolds:</b>	28
<b>2.5. Mechanical and morphological description:</b>	28
2.5.1. Morphological studies:	28
2.5.2. Swelling Test:	28
2.5.3. Deterioration Analysis:	29
2.5.4. Accuracy (%):	29
2.5.5. Stress/strain testing:	30
<b>2.6 Cell culture:</b>	30
2.6.1. Scaffolds preparation for cell viability:	30
<b>2.7. Statistical analysis:</b>	31
<b>CHAPTER 3. RESULTS AND DISCUSSION</b>	<b>32</b>
<b>3.1. FTIR analysis of oxidized Alginate, formulations of bioink and their rheological properties analysis:</b>	32
<b>3.2. Printing and characterization of Gelatin/Oxidized Alginate cryogel scaffolds:</b>	34
<b>3.3. Scanning electron microscope and mechanical results of the selected 2.86% w/v Gelatin/Oxidized Alginate scaffold:</b>	37
<b>3.4. Cell seeding efficiency on Gelatin/Oxidized Alginate scaffold (2.86% w/v):</b>	39
<b>CHAPTER 4. CONCLUSION</b>	<b>41</b>
<b>REFERENCES</b>	<b>42</b>

# List of abbreviations

3D	Three dimensional
AM	Additive Manufacturing
BTE	Bone tissue engineering
DMEM	Dulbecco's Modified Eagle Medium
DD	Degradation degree
ECM	Extracellular matrix
FBS	Fetal bovine serum
FTIR	Fourier transform infrared
Gel	Gelatin
GelMA	Gelatin methacrylamide
GPa	Gigapascals
HAp	Hydroxyapatite
kPa	Kilopascals
MPa	Megapascals
OxAlg	Oxidized sodium alginate
PA	Printing accuracy
SC	Swelling capacity
SEM	Scanning Electron microscopy



# List of Figures

<b>Figure 1.1</b> Bone cells types (Osteocyte, Osteoblast, Osteogenic cell, and Osteoclast) .....	12
<b>Figure 1.2</b> Human bone hierarchical structure .....	14
<b>Figure 1.3</b> Components used in bone tissue engineering .....	15
<b>Figure 1.4</b> Scheme of the 3D bioprinting process .....	24
<b>Figure 1.5</b> Schematic of an extrusion-based bio-printing method .....	25
<b>Figure 3.1</b> FTIR measurements of alginate (-) and oxidized alginate (-). The oxidation reaction-introduced aldehyde groups' vibrational band is shown by the arrow.....	32
<b>Figure 3.1</b> Rheological analysis of gel/OxAlg biopolymer compositions with weight percentages of 3.08%, 2.86%, 2.67%, and 2.50%. (A) damping factor ( $\tan \delta$ ) with temperature, and (B) viscosity versus shear rate (logarithmic scale) at 15 °C.....	33
<b>Figure 3.3</b> Cryogelation was used to create macroporous hydrogel scaffolds for 3D printing using Gel/OxAlg. A 3D structure is printed by ink extrusion, followed by 24 hours of cryopolymerization at -20 °C and the creation of a macroporous hydrogel scaffold after thawing at room temperature.....	34
<b>Figure 3.4</b> The properties of Gel/OxAlg ink-printed scaffolds with concentrations of 3.08%, 2.86%, 2.67%, and 2.50% (1:1) w/v were analyzed. Optical pictures and SEM cross-sectional view micrographs were taken to show the scaffolds just after printing. The swelling capacity of the scaffolds was calculated after 1 and 5 hours, as well as their temporal water absorption and degradation rate in PBS at 37 °C (*#\$ show significant changes related to the 5 hours measurement with $p < 0.05$ ). The relationship between ink concentration, PA, and the mechanical and morphological traits of the resultant 3D-printed scaffolds is summarized in (F) a web chart. The total number of replicates for all experiments is $N = 4$ . All investigations utilized a pH value of 7.4.....	36
<b>Figure 3.5</b> Characterization of the 2.86% w/v (1:1) Gel/OxAlg 3D printed scaffold's structural and mechanical properties. The SEM micrographs were taken after cryogelation and included images of the full-size optical print (A), a top view (B), a cross-sectional view (C), and a magnified view of a representative area (D). The histogram data was based on four cubic samples measuring 2 x 2 x 1 mm in (E) depicts the dispersion of averaged pore diameter. The SEM image was examined using ImageJ's binary grayscale surface	

analysis. The elastic moduli were graphed against the scaffold's mass loss after it had been incubated in PBS for durations of 1, 7, 14, and 21 days (F) and stress-strain behavior (Inset: magnified curves at lower strain values) in (G). Significant differences between the sample and other samples are indicated by a (\*) when  $p < 0.05$ .....38

**Figure 3.6** Using NIH/3T3 fibroblast cells, 3D printed 2.86% Gel/OxAlg cryogels were characterized in vitro. (A) Illustrations of the cryogels following cell seeding at days 1, 7, 14, and 21 using live/dead staining. The color green denotes fluorescence in living cells, while red represents fluorescence in dead cells. Cell nuclei are seen as blue (Hoechst 33342). The combined column of images displays live/dead staining with Hoechst overlaid. Individual stained cells are seen in zoomed images from the specified locations. With the program Zen light, color enhancement was made for improved visibility (maximum intensity). 100  $\mu$ m is shown by the scale bar. (B) Quantitative study of the cell viability on days 1, 7, 14, and 21.....40

# Chapter 1- INTRODUCTION

This chapter provides essential background related to biomaterials in the context of 3D printing for bone tissue engineering. The first part of the chapter covers the basic composition, structure, and mechanical properties of natural bone. The second part discusses different types of natural and synthetic biomaterials used to fabricate scaffolds for bone tissue engineering. The various factors related to physical properties and morphology, as well as the different fabrication techniques, are also discussed in detail.

## **1.1. Human Bone:**

### **1.1.1. The function of bone in the body:**

Bones are an amazing, multi-layered organ system that acts like a shield to protect the internal organs of the body, including brain, heart and lungs that prevent the organs from collapsing into each other. Bones are not only involved in movement, but also serve as the main storage for calcium and other minerals and ions. In addition, the bones are the main source of red blood cells, which are formed in the marrow of the long bones. The bone should be a natural, durable substance that serves as a protective and structural system, but some bone diseases and trauma can affect the bone's ability to heal itself [1,2].

### **1.1.2. Bone development process:**

Bone has a strong capacity for regeneration and can heal itself without external assistance. Bone tissue is constantly modified as a result of the coordinated actions of bone cells, which include bone resorption by osteoclasts and bone creation by osteoblasts, with osteocytes acting as mechanosensors and orchestrators of the bone remodeling process (Figure 1.1).

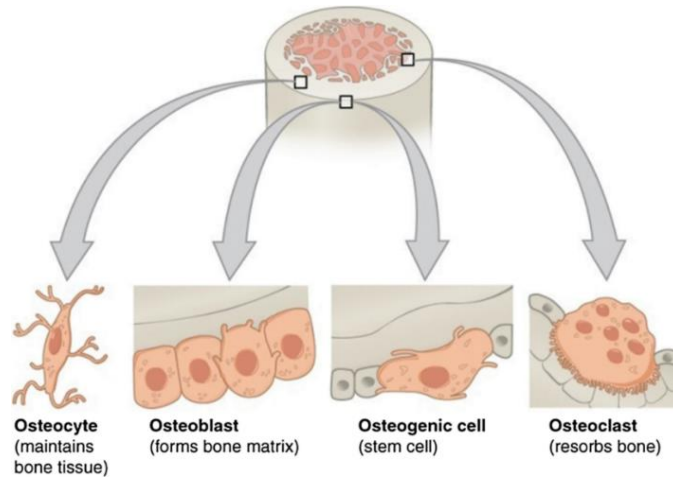


**Figure 1.1** Bone cells types (*Osteocyte, Osteoblast, Osteogenic cell, and Osteoclast*) [3]

### 1.1.2.1 Osteoblasts:

Osteoblast cells are the first to create bone tissue. They are mononuclear cells that secrete extracellular matrix proteins to produce new bone matrix, including osteocalcin, sialoprotein, osteonectin, osteopontin, fibronectin, and vitronectin. Osteoblasts are polarized cells with nuclei at boundaries that deposit at the junctions next to the formation of bones, such as the periosteum (external surface) and bone marrow (internal surface). They possess an elaborate organelles apparatus that is typical of cells involved in protein synthesis. Additionally, tissue mineralization is changed by alkaline phosphatase production. High alkaline phosphatase levels are expressed during osteoblast differentiation.

### 1.1.2.2. Osteocytes:

The majority of bone cells, known as osteoclasts, are found in adult bone. They are mature osteoblasts that are enclosed in demineralized or osteoid bone matrix. They have a single nucleus and a form of mitochondria h an endoplasmic reticulum and are trapped in tiny holes in the bone matrix. This morphology is specifically employed to measure and maintain the concentration of bone minerals within the bone matrix through small channels. Osteogenic cells, which exhibit high levels of mitotic activity and are undifferentiated, are the only bone cells that divide. Immature osteogenic cells can be found in both the marrow and the deep layers of the periosteum. As a result of differentiation, they develop into osteoblasts.

### **1.1.2.3. Osteoclasts:**

Bone resorption is the primary role of osteoclasts. Osteoclasts are enormous multinucleated cells derived from the differentiation of monocytes and macrophages. They can be found on the surface of the bone as well as in parts of the bone that are unneeded, diseased, or ancient. Osteoclasts (bone resorption) and osteoblasts (bone formation) work in harmony to preserve healthy bone (bone deposition). This ongoing process regulates the growth and remodeling of bones [3].

### **1.1.3. Bone structure and composition:**

Bone is a fundamental skeletal network of all vertebrates. It is made up of hydroxyapatite, type I collagen, organic matrix, non-collagen bone proteins, and lipids. Concerning several aspects, such as gender, age, and a person's state of health, the relative amount of organic and inorganic components changes. The collagenous matrix's incorporation of hydroxyapatite gives it stiffness and shape, both of which are necessary to safeguard and sustain physiological function. However, bones serve additional crucial roles in addition to supporting the body [4, 5]. The most significant aspect of bone is that it is a highly vascularized connective tissue that participates in remodeling and repair during a person's lifetime. When it comes to bone turnover during childhood, formation outpaces repair at a very high rate. After reaching adulthood, bone net loss begins when bone synthesis and repair are in equilibrium [6]. The collagen matrix, bone size and shape, density, and bone turnover rate can all be used to predict the mechanical properties of bones. These factors can be flawed, leading to osteopetrosis, osteopetrosis imperfect and Paget's disease of the bones, among other disorders [7]. Every biological tissue, including bone, has a complex hierarchical structure that ranges from macro to nanoscale. Figure 1.2 illustrates this structure. Different building block arrangements exist on each scale in bone, supporting and influencing both macro and nanoscale. These fragile blocks' linkage with hydroxyapatite crystals at the nanoscale exhibits a superb fusion of mechanical qualities and various biological activities. The extracellular matrix of the bone communicates topographical and chemical information to the cells in bone ultra-porous geometry [8,9]. Bone tissue is separated into two categories on a macro scale: cortical bone and trabecular bone. Despite having a similar composition, both bones. Due to its extreme density and more solid porous channels, the cortical bone holds 80% of the body's skeleton's mass, which is higher than that of trabecular bone [10]. The remaining 20% of the mass is made up of trabecular or sponges bone, which has a spongy or honeycombed shape in the interior bone part and is extremely porous and strongly linked. Stress directions significantly affect the orientation and density of the trabecular. Overall, the bone's mass,

geometry, and structure, rather than its chemical makeup, determine its strength [11].

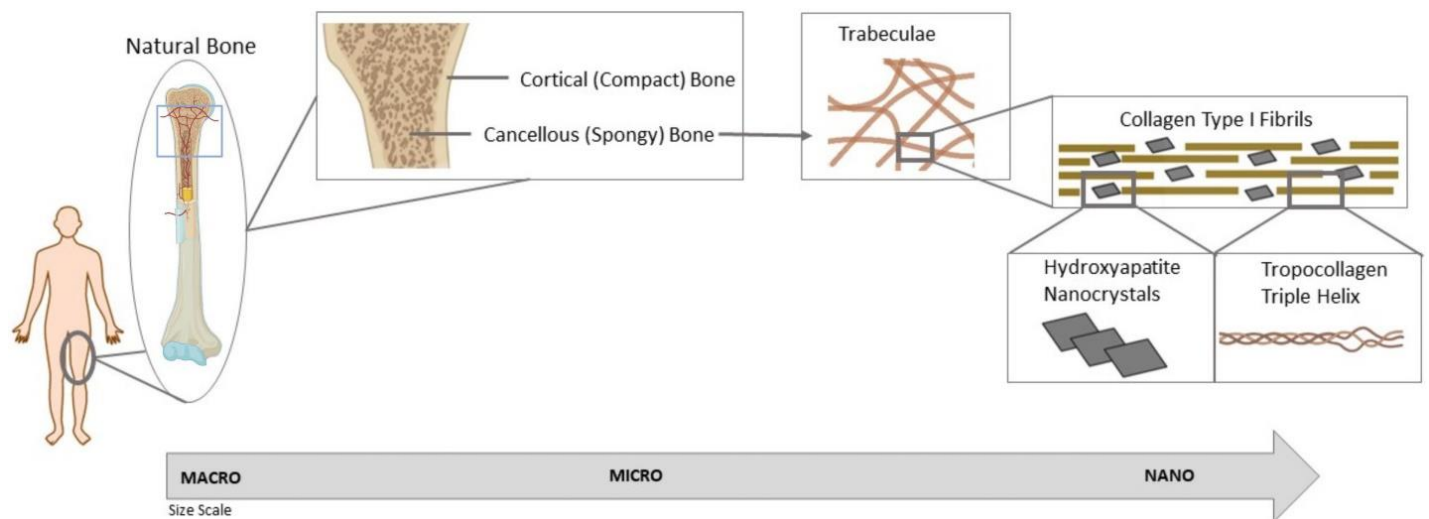


*Figure 1.2 Human bone hierarchical structure [8]*

Natural bone's mechanical characteristics are highly influenced by an individual's age and body part. Additionally, the entire bone or the isolation of certain components from the bone's structure is examined for mechanical properties. Young's modulus and stress yield are primarily employed to gauge the anisotropy of natural bone. The mechanical properties of bone Tensile strength (104–121 and 120–140 MPa, Yield strength (20–193 MPa and 2–80 MPa), and Elastic modulus (4–30 GPa and 0.2–2 GPa) are reported for cortical bone and Trabecular bone, respectively [12]. To examine its mechanical capabilities, the trabecular bone's porous nature, and trabecular arrangement are used. Because of the high level of complexity and data variance, mechanical properties in bone microstructure cannot be predicted accurately by mathematical models [12,13].

## 1.2. Bone Tissue Engineering (BTE):

One of the central areas of regenerative medicine is the engineering of bone tissue (BTE). Although human bones are known for their capacity for self-healing, lengthy bone abnormalities cannot be repaired using regenerative techniques. Bone tissue engineering (BTE) has been proposed to overcome the challenges. BTE is also utilized in a wide range of novel treatments for contemporary medical issues like osteoarthritis, dentistry, osteoporosis, and bone cancer. Bone tissue engineering aims to stimulate new tissue repair and regeneration by utilizing a synergy of cells, scaffolds, and signals. Bone tissue engineering techniques are

shown in Figure 1.3 [14]. Cells and signals are carried via a scaffold constructed from biomaterials. Even with the introduction of unique patient-specific therapeutic therapies for damaged tissue, biomaterials utilized for bone regeneration have shown a great deal of promise in clinical use. Before everything else, the materials suitable for the production of bone tissue should exhibit the three fundamentals. The first process is called Osteoinduction which defined is as the capacity to draw in progenitor cells and encourage differentiation into the osteoblastic lineage. Second, Osteoconduction that to supports of surrounding tissue and encourage the production of bones. Third, the implanted material must be physically and functionally integrated with the nearby bone known as Osseointegration [15].

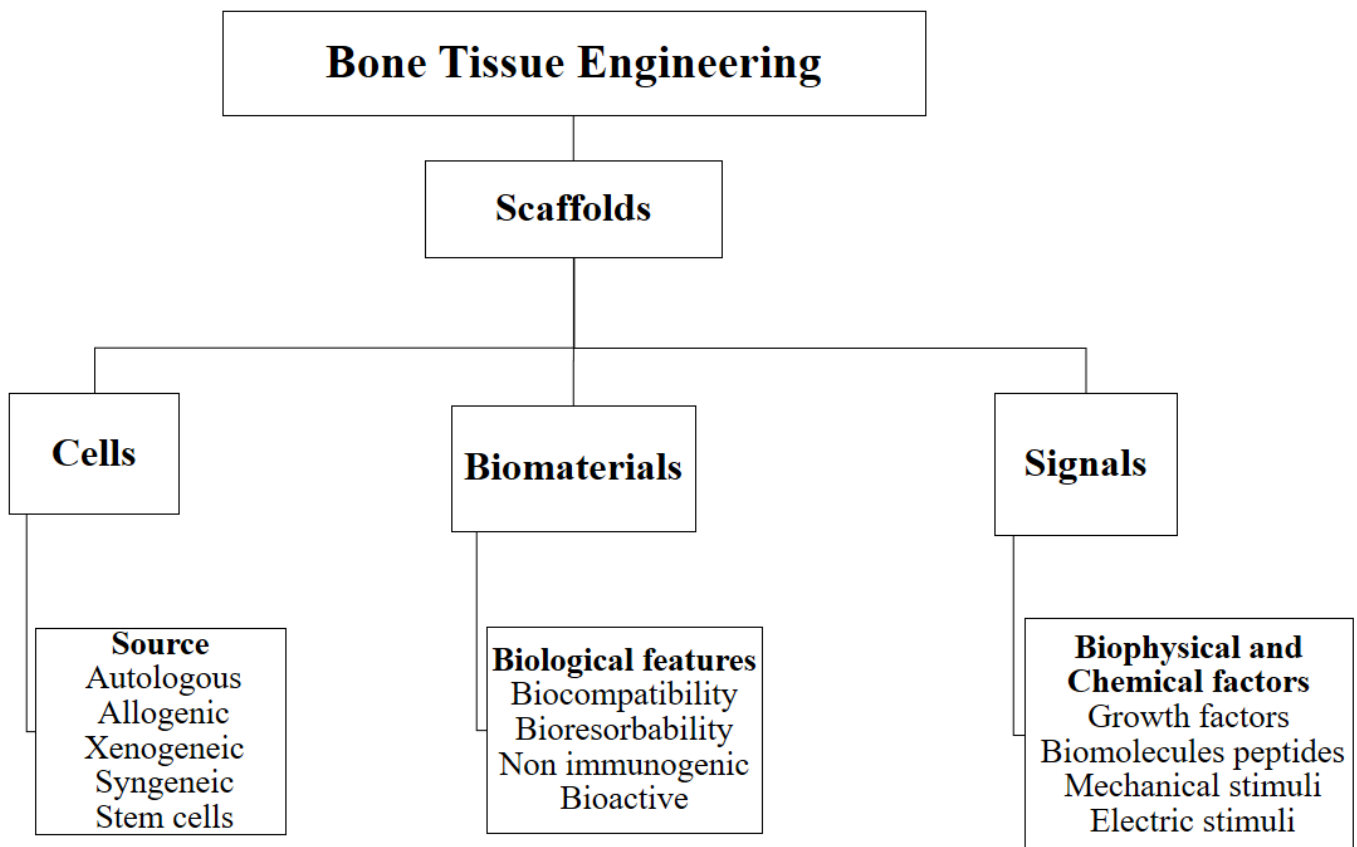


*Figure 1.3 Components used in bone tissue engineering. [14]*

### **1.2.1 Scaffolds in Bone Tissue Engineering (BTE):**

Scaffolds are an essential part of bone tissue engineering, also known as 3D structure, which mimics bone's natural ECM structure. The 3D scaffolds provide a platform for bone cells to grow, multiply, and differentiate into tissue. Hydrogels are used to prepare scaffolds for cell culture and tissue engineering due to their tissue-like water content, injectability, and adjustable properties. In the traditional bone tissue engineering procedure, bone cells are either seeded or cell-laden with scaffolds to promote bone regeneration. Most experts believe that improving scaffold properties will be critical to the future of BTE [16,17].

A variety of factors influence the performance of scaffolds. Biomaterials (hydrogels), composite porosity, permeability, crosslinking and mechanical strength are examples of such properties. These variables cannot be accurately controlled using standard fabrication techniques. For this reason, several multidisciplinary investigations have been conducted on this topic, ranging from design and modeling, material processing, and post-treatment, to in vitro and in vivo biological evaluations[16-19]. These functions and features are explored in more detail in the following subsections

### **1.2.2. Biomaterials used for Scaffolds Fabrication:**

To create three-dimensional (3D) scaffolds, numerous materials have been used in the tissue engineering field. The choice of materials depends on their biocompatibility, cell growth support, mechanical strength, and biodegradability. Collagen, a biological polymer, and natural ceramic elements are all components of bone tissue. The basic objective of bone tissue engineering is to use scaffolds as implants that disintegrate over time without having any deleterious consequences on the body. Therefore, the scaffold material needs to be biocompatible and have a variety of characteristics to enable the growth of cells into the ECM [19, 20].

In bone tissue engineering, there are two different types of biomaterials. Gelatin, alginate, chitosan, hyaluronic acid, agarose, and collagen are examples of natural biomaterials. Synthetic materials include PMEMA, PVA, PNIPAM, PEG, PLA, PGA, and PCL [21–23]. Natural biomaterials have viscoelasticity, low inflammatory response, and biodegradability. The first essential component is collagen, which is most frequently utilized in bone tissue creation because it promotes mineralization and enzyme-mediated biodegradability [20]. When compared to other biopolymers, silk fibroin demonstrated a high mechanical strength. Due to its flexibility and tensile strength, silk fibroin is used in load-bearing scaffolds in bone tissue



engineering. By creating hierarchical structures via ice-templating, the porosity of the scaffolds may be managed. It has greater mechanical qualities, is more biodegradable, and more closely resembles the bone ECM matrix to support cell proliferation when contrasted to other natural biomaterials [24]. Next, alginate is a mechanical biomaterial that is very flexible and inherently cytocompatible. Due to controlled situ gelation during scaffold bioprinting, it is the ideal candidate for bone tissue engineering. Alginate exhibits enhanced characteristics in 3D bioprinted scaffolds when combined with other appropriate components. For optimum cell survivability and function, alterations to natural alginate hydrogels are required to produce gels that resemble the physiological environment of encapsulated cells. Several cell types, including corneal endothelial cells, hepatocytes, fibroblasts, mesenchymal stem cells, adipose stem cells, and human osteoprogenitors, have previously been shown to be cytocompatible with oxidized alginate gels in particular. By replacing the original components with hydroxyapatite (HAp), the scaffold's mechanical qualities were improved. One naturally occurring substance, chitosan, shares the same structural characteristics as the glycosaminoglycans, which make up the majority of the ECM. It has been employed in scaffolds for bone tissue engineering using nanoparticles. A perfect biomaterial for bone tissue engineering, its structural characteristics enable cell adhesion, differentiation, and ingrowth [25-27].

Gelatin is a suitable biomaterial for the engineering of bone tissue since it has a similar composition to collagen but has been denatured. Scaffolds made of gelatin resemble the 3D extracellular matrix in living things. It demonstrated strong biocompatibility and biodegradability. Gelatin has been combined with various biomaterials, such as nHA or titanium, in 3D bioprinting to create scaffolds. For the creation of scaffolds, various crosslinking techniques are typically used. The porosity structure and superior biocompatibility of scaffolds made of gelatin were evident. The resulting porous scaffolds have enabled cell growth and proliferation, which has led to the development of osteoblasts. Additionally, adding methacrylate groups to gelatin produces Gelatin methacrylamide (GelMA), which is a perfect physicochemical candidate for extracellular matrix (ECM). Gelatin methacrylamide (GelMA) is a stable substance at body temperature that improves cell viability and can create vascular networks that are useful for cartilage regeneration. The other abundant natural element is HAp, which is likewise similar to bone tissue and the organic component of the bone's hierarchical structure. It has been employed as a bioceramic filler for teeth or bone, covering for implants, and bone hard tissue repair [28].

The HAp has been utilized extensively to treat hard tissues; typical applications include bone repair, bone augmentation, coating of implants, and functioning as filler in bone or teeth. Normal HAp ceramics' low mechanical strength, on the other hand, typically limits their employment to light load-bearing applications.

Calcium and phosphate ions make up the majority of HAp, which means that it has strong biocompatibility, bioactivity, and affinity. Since it has no toxicological effects, it has been tested on animals like goats, dogs, and baboons. A very ideal choice for bone tissue engineering, HAp biomaterial is bioresorbable, has a pore structure, is mechanically appropriate, and is bioactive [29]. In contrast, the physical and mechanical characteristics of synthetic biomaterials can be predicted based on the conditions of synthesis. Impurities are more easily controlled in synthetic materials than in natural polymers, which is their main advantage. As a result, it lowers the levels of toxicity risk [30, 31].

### **1.2.3. Crosslinking in the 3D Printed Scaffolds:**

In BTE, crosslinking significantly affects the biomechanical characteristics of scaffolds and the printability of hydrogels by creating a strong network in the polymeric matrix. For different hydrogels used in bioprinting, numerous crosslinking techniques have been developed. These techniques include physical, chemical, and enzymatic crosslinking. Hydrogels that are chemically crosslinked make use of crosslinking agents, either molecule or ionic, to interact with the polymeric chains in a covalent or coordinative way. This results in the creation of strong and long-lasting hydrogel-network structures. In contrast, hydrogels physically crosslinked depend on the activation of chain crosslinking by external stimuli like light or temperature. While physically crosslinked hydrogels are useful in treating small voids in bone defects due to their mild gel-forming conditions, chemically crosslinked hydrogels are better suited for treating larger and more difficult bone defects. Hydrogels that are physically crosslinked come into existence when molecules interact reversibly, for example through hydrogen bonding, ionic interactions, hydrophobic/hydrophilic interactions, entanglements of polymer chains, crystallization of stereo complexes, coordination of metal, and the stacking of  $\pi$ -bonds. Physical crosslinking doesn't involve the use of chemical crosslinking agents, which makes physically crosslinked hydrogels a better option for biomedical applications due to their ability to prevent potential cytotoxicity. They are also able to self-heal at room temperature, are injectable, and can respond to environmental stimuli [32-34].

When compared to physically crosslinked hydrogels, chemical crosslinks are inherently robust and long-lasting couplings created by covalent bonding between polymeric strands. Enzyme function, polymerization through free-radicals, the Schiff-base chemical reaction, the Michael addition process, the formation of oximes, and the "click" reaction of Diels-Alder are some instances of this. Chemically crosslinked hydrogels have outstanding mechanical properties and a controllable degradation profile, making them more stable (in a

physiological setting). [33-35].

Enzymes are extremely effective and only need a small amount of energy to work; they speed up reactions without using any of their energy. The number of substrate molecules that an enzyme converts into products per unit of the enzyme sometimes referred to as a turnover number, determines the effectiveness of the enzyme ( $k_{cat}$ ). Because they guarantee the conversion of a certain kind of substrate into products, enzyme-based reactions are very efficient. To create biomimetic hydrogels for bone tissue engineering, numerous enzymes have so far been investigated. Combining several crosslinking strategies is another useful tactic that can be a useful replacement for traditional approaches. Even though up to now, this method has rarely been explored in BTE programs, a combination of physical and chemical crosslinking may be a viable choice [36,37].

#### **1.2.4. Morphology of scaffolds and its effect on tissue development:**

The porosity and pore dispersion of the scaffold allow inappropriate infiltration and ingrowth of cells. These porosity properties provide the cellular network and nutrient-associated pathways for transport, adhesion, cell signaling, and proliferation in a three-dimensional environment [38, 39]. As a result, the different pore sizes of scaffolds have had an experimental impact on cell behavior. Fluid flow through a bone skeleton is important because it has the potential to generate living tissue. Successful BTE depends on the ability of the scaffold to allow diffusion of nutrients and removal of waste from the regenerative site and to provide a suitable mechanical environment. Scaffold fabrication requires knowledge of pore size, pore volume, interconnectivity, shape, and pore dispersion, which can affect both *in vivo* and mechanical performance. Pore size and porosity are highly dependent on the crosslinking processes [40-42]. The pore size must be in a critical size range. Nevertheless, the optimal pore size is still a controversial issue in the field of bone tissue engineering. Pore sizes can be divided into two categories: Micropores ( $< 100 \mu\text{m}$ ) and Macropores ( $> 100 \mu\text{m}$ ). Pore size range affects scaffold permeability, cell migration, and differentiation. From the micropores point of view, a small pore size decreased the permeability of the scaffold and cell migration. On the other hand, macropores improve nutrient flow into the scaffold, remove waste fluid, and promote cell growth and vascularization through the pores. Different pore sizes resulting from different types of the crosslinking process, including neovascularization (ca.  $5 \mu\text{m}$ ), fibroblast ingrowth (ca.  $5\text{--}15 \mu\text{m}$ ), hepatocyte ingrowth (ca.  $20 \mu\text{m}$ ), and adult mammalian skin regeneration needing (ca.  $20\text{--}125 \mu\text{m}$ ) sizes, are documented [43–45]. Numerous applications have been hindered by hydrogels' micropores, poor

interconnectivity, and toxicity because these factors limit cell viability, cell spreading, and nutrient transfer [46].

At the macroscopic level, scaffolds must accurately reproduce the mechanical forces to which cells are subjected during adhesion. Cells may develop into different morphologies if the scaffolds are unable to maintain their mechanical stiffness. There is a relationship between the porosity, pore size, shape, orientation, and mechanical properties of the scaffold. However, as porosity increases, mechanical strength decreases, and cell differentiation may be compromised, especially with larger pore sizes. Therefore, a compromise should be made between structural properties and biological considerations. Mechanical properties of scaffolds include modulus of elasticity, compressive strength, and fatigue strength. The optimal scaffolds for bone cell ingrowth have a tensile strength of 50-151 MPa, a compressive strength of 100-230 MPa, and a modulus of elasticity of about 7-30 GPa. These results indicate that the porosity of the scaffold should exceed an average pore size of 150  $\mu\text{m}$  [17,18].

In addition, the surface of a scaffold implanted in the body first comes into contact with the surrounding tissue. It is best to use large surface scaffolds with topographical and chemical properties. In response to the host response, the surface properties are now modified by using chemical or biological elements [47]. Although many types of properties, such as mechanical, can be improved, biocompatibility is always the central issue. In this way, cell development, differentiation, and proliferation are promoted. Scaffolds can be mechanically improved by using natural fibrils. Collagen, fibronectin, and other growth factors (bFGF and ECF) are examples of adhesive proteins used to promote biocompatibility by adhering electrostatically and covalently to the surface of biomaterials [48,49].

Multiple techniques have been developed to fabricate 3D fabric scaffolds with macroporous structures, for instance 3D printing, polymer phase separation, freeze-drying, porogen leaching using salt or polymeric microspheres, and gas foaming [19, 50]. However, despite the availability of various technologies for generating macroporosity in 3D scaffolds, there are still significant challenges that must be overcome before they can be widely used for tissue engineering purposes. Firstly, most of the existing techniques only enable the fabrication of scaffolds with predetermined, fixed porosity. Nonetheless, different sizes and densities of macropores are beneficial at different stages of tissue growth. While low porosity is desirable for providing initial structural stability and supporting grafted cells, higher porosity is necessary over time to enable efficient ingrowth of blood vessels and nutrient diffusion, as well as to create enough space for cell proliferation and matrix formation. Biodegradable polymer scaffolds can increase porosity over time, but there is no direct control over the timing and extent of macropore formation that aligns with the stages of

tissue formation. Secondly, current methods for producing macroporous scaffolds often involve manufacturing conditions that are too harsh for cell survival, such as high temperatures, high pressure, nonphysiological salt concentrations, or the use of organic solvents. Consequently, cells can only be seeded onto pre-fabricated macroporous scaffolds, leading to low cell seeding efficiency and uneven distribution. One technique used in tissue engineering is called "cryogelation." [16-19,51].

### **1.2.5. Cryogelation:**

With the advancement of technologies, crosslinking agents for better structure and porosity are the main points in scaffold fabrication. Cryogelation, an environmentally benign method that may create hydrogels with a highly porous structure without using harmful solvents, has recently been made available as an alternative crosslinking technique [52]. In the process of cryogelation, the solution reaction is started in a water-cooled chamber below zero degrees Fahrenheit. Because the polymer's polymer, monomers, and crosslinker are released as the solution begins to freeze, water ice crystals and macrospores are produced [53,54]. In gelatin, cryopolymerization takes place in ice crystals, resulting in a massive, thick cross-linked polymer structure. In the gel, thawed ice crystals leave behind a significant and continuously interconnected macroporous structure [55]. The Cryogels, also known as cryo-hydrogels, are connected in a three-dimensional (3D) network structure that resembles a sponge. Cryogels have the desired biocompatible and physically robust structures for cell development, which is another benefit. In recent years, many different biomedical applications, such as drug administration, tissue engineering, and bioseparation, have been reported for these advanced hydrogels or cryogels

### **1.2.6. Stability and integrity of scaffold:**

The degradation of scaffolds can be caused by biological, chemical, or physical processes that are mediated by biomolecules including enzymes. Polymeric materials do not biodegrade on their own; they must first have hydrolytically or enzymatically sensitive connections broken. Degradation rates are influenced by a variety of polymer features, including chemical structure, the existence of weak bonds, hydrophilicity or hydrophobicity, and crystalline/amorphous morphology. The biodegradable scaffold eventually disintegrates, allowing for the replacement of the structure with newly generated tissue after a certain time. In the course of the degrading process, the internal structural bonds of the polymeric scaffolds broke broken, causing the molecular mass to decrease. Non-biodegradable polymer scaffolds, such as poly (methyl methacrylate)

(PMMA), are available for patients who require long-term or permanent support [56,57]. PMMA is used in hip and knee replacement surgery as bone cement.

### 1.2.7. Scaffold fabrication techniques:

Fabricated scaffolds serve primarily as temporary 3D environments for cell proliferation, ingrowth, and differentiation. Regarding the manufacturing of scaffolds, a variety of technologies are available, including 3D bioprinting, electrospinning, freeze-drying, phase separation, gas foaming, and salt leaching procedures [19, 58]. Table 1.1 List the benefits and drawbacks of the various scaffold fabrication

**Table 1.1 : Different techniques for fabrication of scaffolds with benefits and limitations [19, 58]**

<b>Methods</b>	<b>Benefits of the technologies</b>	<b>Limitation Bioprinting scaffold fabrications methods</b>
<b>3D Bioprinting</b>	<ul style="list-style-type: none"> <li>• Less time is needed to construct 3D scaffolds</li> <li>• Scaffold materials can be printed using high-concentration ingredients.</li> </ul>	<ul style="list-style-type: none"> <li>• Costly 3D bioprinting</li> <li>• Insufficient bioink resources</li> </ul>
<b>Electrospinning</b>	<ul style="list-style-type: none"> <li>• Printing of nanometer-sized scaffolds and an easy method for producing scaffolds</li> </ul>	<ul style="list-style-type: none"> <li>• Less mechanical strength and the usage of organic materials</li> <li>• Which is detrimental to cells</li> </ul>
<b>Freeze-Drying</b>	<ul style="list-style-type: none"> <li>• The method didn't make use of solid porogen</li> </ul>	<ul style="list-style-type: none"> <li>• Time-consuming fabrication</li> <li>• Organic material use which harmful to the cell</li> <li>• Small porosity</li> </ul>

<b>Phase Separation</b>	<ul style="list-style-type: none"> <li>• This procedure can be used in conjunction with other techniques because it does not utilize solid porogen.</li> </ul>	<ul style="list-style-type: none"> <li>• Use of organic materials</li> <li>• Less porosity</li> </ul>
<b>Gas Foaming</b>	<ul style="list-style-type: none"> <li>• No organic compounds were used in the procedure.</li> </ul>	<ul style="list-style-type: none"> <li>• The scaffolds are made using high pressure with no pore size control.</li> </ul>
<b>Salt leaching</b>	<ul style="list-style-type: none"> <li>• A simple method that allows for regulated composition and porosity</li> </ul>	<ul style="list-style-type: none"> <li>• Less mechanical properties and the use of hazardous organic materials for cells</li> </ul>

A 3D salt leaching can be easily made using the salt leaching approach. A polymer solution that was thermally generated and uniformly mixed salt served as the porogen in the process. A salt matrix and polymer are all that is left after the solution evaporates. After that, a porous matrix was submerged in water to dissolve the salt crystals. Making a porous scaffold with this technique is inexpensive [59].

The second procedure is the freeze-drying method, which is utilized to incorporate a macroporous sponge matrix into the scaffolds. It employed ice crystals as a porogen to create porous structures that allowed the ingrowth of cells inside a three-dimensional environment. Similar to this, the Gas Foaming process is employed in the creation of macroporous scaffolds utilizing high-pressure carbon dioxide. When the gas is applied, it saturates the ceramic/polymer combination because it is applied at room temperature. As a result of thermodynamic instability, which results in the creation of pores in the matrix when the CO<sub>2</sub> pressure is reduced, the gas solubility rapidly decreases [60].

Due to its use in reconstructive surgery, electrospinning has attracted attention in recent decades. The procedure for creating fibrous mats made of biodegradable polymers is straightforward and flexible. The ECM of living tissue is replicated by the micro-nanoscale electrospinning fiber. While a high voltage is delivered at the tip during electrospinning, the fiber mat is collected at the collector. In addition to tissue engineering, there are many other uses as well, including medicine delivery and growth factors. Additionally, there are some limitations on both natural (collagen, fibrinogen) and synthetic (PLA, PCL, PLGA) materials, which is another disadvantage of this method. Another option is a thin, micrometer-scale fiber with a few thin

layers that are inappropriate for extracellular matrixes that are naturally that size [61].

### 1.2.8. 3D bioprinting in bone tissue engineering:

A wide range of applications in tissue engineering and regenerative medicine tailored to the needs of individual patients have made additive manufacturing, often known as 3D printing, one of the most revolutionary technologies in the modern world. The extracellular matrix (ECM), which gives cells a platform for proliferation and differentiation like human tissue, is specifically imitated in 3D scaffolds that are created using a 3D printer. Due to the current organ shortage and other treatment approaches' failure rates to save human lives, 3D scaffolds have been illustrated [62,63]. Figure 1.4 showed this 3D scaffold building procedure. When compared to alternative ways of fabricating scaffolds, 3D bioprinting offers several benefits, such as the ability to create complex microstructures with high precision and repeatability, control over the sizes and shapes of the pores, which results in good mechanical properties, and honeycomb-like structures with morphological characteristics comparable to those of cancellous bone structures found in nature [64,65].

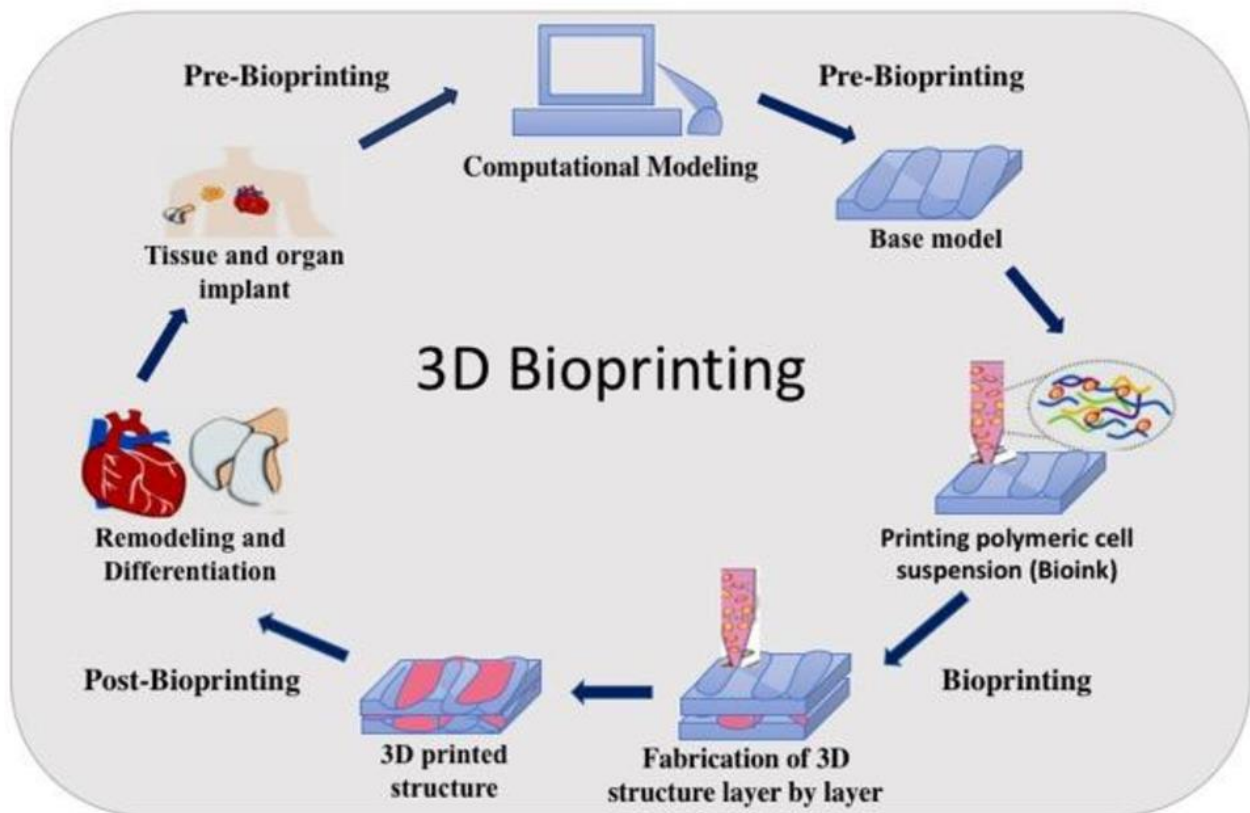
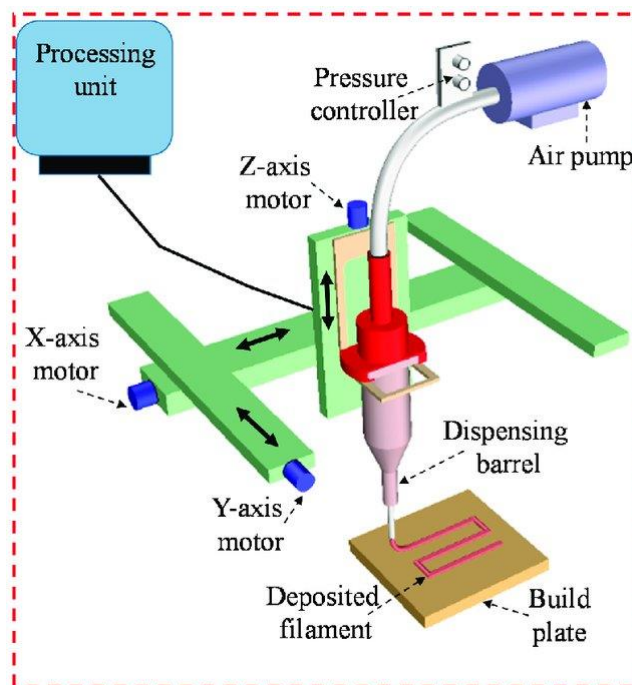


Figure 1.4 Scheme of the 3D bioprinting process [65]



Despite the significance of 3D bioprinting, it is preferable to be aware that this technology is still in its infancy. Currently, research is being done to create bioink made of appropriate biomaterials for this use. For bioprinting, the biomaterials need to have the right rheological, mechanical, and degrading characteristics. Limitations are a process of AM technologies. It is important to understand the differences between inkjet-based, extrusion-based, and laser-assisted 3D bioprinting techniques to overcome these constraints [66-68]. The first bioprinter was an inkjet printer that had been modified. A thermal actuator or a piezoelectric actuator has been used by this bioprinter. These actuators use temperature or voltage variations to eject materials and cell suspension. This method has the drawback of being unable to continue flowing the materials for the desired shape [69].

An air pump is used to continually push the bioink through the print head tip in the extrusion-based 3D bioprinting technique, as shown in Figure 1.5 to alleviate this issue. Through the use of these procedures, a variety of biomaterials and cell types can be produced. The key differences between a bioprinter and an inkjet printer are that the latter can print several types of biomaterials, while the former is less expensive, less prone to nozzle clogging, and less likely to cause cell death while printing [70].



**Figure 1.5** Schematic of an extrusion-based bio-printing method [70]

### **1.3. Thesis statement:**

We hypothesized that a combination of natural biopolymers and their derivatives at certain ratios, namely, gelatine and oxidized alginate, can provide valid core precursor material, suitable for 3D printing and further formation of the scaffolds via cryogelation. Furthermore, we speculated that the mechanical stability, as well as the degradation rate of the 3D macroporous structure, can be controlled via the concentration of the polymer content in the ink, while maintaining the same level of low cytotoxicity. The resulting 3D-printed scaffold provided a suitable environment for the successful seeding of the cells and their enhanced growth development and evolution into mature tissue.

### **1.4. Aims and Objectives:**

#### **1.4.1. Aim:**

In bone tissue engineering, the use of hydrogel scaffolds with large pores has demonstrated advantages. To bridge the gap between the constraints of pore diameter and the manufacture of hydrogel scaffolds through extrusion-based 3D printing, we propose a solution in this study. By optimally formulated Gel/OxAlg-based ink, 3D printing technology, and cryogenic synthesis, we aimed to produce biodegradable scaffolds with high porosity and exceptionally large pores for implementation in tissue engineering.

#### **1.4.2. Objectives:**

Achievement of the aim has been conducted via the following objectives:

- Creation of an ink made from Gel/OxAlg that is appropriate for use in 3D printing
- Fabrication of macroporous Gel/OxAlg-based scaffolds via cryogelation.
- Characterization of mechanical properties and morphology of 3D printed scaffolds.
- Demonstration of biocompatibility and stability of the scaffolds in vitro.

# CHAPTER 2. METHODS AND MATERIALS

## 2.1. Chemicals:

All of the following items were bought from Sigma-Aldrich: porcine skin gelatin (strength-300, Type A), sodium periodate (with a purity of 99%), ethylene glycol (50% weight in water), glutaraldehyde solution, sodium alginate (with a purity of 99%), and various cell culture reagents such as Fetal bovine serum (FBS), Dulbecco's Modified Eagle Medium (DMEM), Trypsin EDTA (0.25%), and an antibiotic antimycotic solution.

## 2.2. Synthesis of biopolymer and formulation of ink:

The oxidation process of sodium alginate used in this experiment involved periodate cleavage, which produces two aldehyde groups. The procedure was modified from previous reports [73], and to achieve a 10% conversion, 0.0227 mol of sodium alginate was dissolved in 165 ml of ultrapure water, and 0.00227 mol of sodium periodate was added in darkness. The reaction was quenched with ethylene glycol, and the solution was precipitated in ethanol with NaCl-containing water three times. The resulting product, named OxAlg, was analyzed using FTIR and stored at 4°C.

To make the bioink, an 8% w/v aqueous solution of OxAlg was mixed with an equal volume of gelatin solution, and glutaraldehyde was added to the cool ultrapure water dilution. Ink solutions were prepared by adding 60%, 50%, 40%, and 30% of the solution, resulting in 3.08%, 2.86%, 2.50%, and 2.67% ink solutions, respectively. The ink solutions were mixed thoroughly for 2 minutes at room temperature before being loaded into a printing tube for 3D printing.

## 2.3. Shear thinning properties:

To evaluate the shear thinning properties of the hydrogels, a rheometer (Anton Paar, MCR302) with 20 mm diameter parallel plates was utilized. The measurements were conducted at 15°C with shear rates ranging from 0.1 to 100 s<sup>-1</sup> using a rotational test to examine the relationship between viscosity and shear rate in a flow curve. The temperature dependence of the storage modulus G' and the loss modulus G'' was

determined using an oscillatory test, where the hydrogels were exposed to a heating rate of  $1.01\text{ }^{\circ}\text{C}\cdot\text{min}^{-1}$ , a constant shear strain ( $\gamma$ ) of 1%, and a frequency of 1 Hz by calculating the Tan ( $\delta$ ) ratio.

## **2.4. 3D printing of Scaffolds:**

Using a BIOX 3D printer manufactured by CELLINK in Sweden, scaffolds were produced while maintaining temperature control through a temperature-controlled print bed and printhead. The scaffold was constructed by sequentially depositing fifteen layers onto a glass substrate at 10-15  $^{\circ}\text{C}$  using a 27G gauge needle and a syringe. The scaffolds were printed at a uniform speed of  $5\text{ mm}\cdot\text{s}^{-1}$  and an extrusion pressure of 60-75 kPa to ensure uniform hydrogel fibers, with pressure varying based on ink composition. Cryogelation occurred by placing the scaffolds at  $T = -20\text{ }^{\circ}\text{C}$  for 24 hours after printing. Subsequently, the scaffolds were rinsed with water and lyophilized for 24 hours before being stored long-term at  $4\text{ }^{\circ}\text{C}$ .

## **2.5. Mechanical and morphological description:**

### **2.5.1. Morphological studies:**

To conduct morphological assessments of the 3D printed scaffolds, electron scanning microscopy was utilized with a JSM-IT200 (LA) model. Prior to imaging, all samples underwent a lyophilization process lasting 24 hours, and a 7 nm gold coating was applied. Each image was subjected to a 5 kV accelerating voltage.

### **2.5.2. Swelling Test:**

In order to determine the swelling capacity, the freeze-dried scaffolds were assessed by placing them in a 10 mM PBS solution and allowing them to sit at room temperature for 60 and 300 minutes. After removing any excess water, the swollen scaffolds were weighed. The swelling capacity was then computed using Equation 1 [72]:

$$\text{Swelling capacity \% (SC)} = \frac{W(t) - W(0)}{W(0)} \times 100\% \quad (1)$$

Where  $W(0)$  is the sample's dry weight and  $W(t)$  is the sample's weight at each incubation time point.

In order to assess the weight variation over a period of time, freeze-dried specimens were submerged in deionized water for a duration of 14 days while kept at 37°C. After specified intervals, the specimens were taken out of the water, dried to remove excess water on the surface, and weighed. The percentage rise in water absorption was determined utilizing the identical formula (1).

### 2.5.3. Deterioration Analysis:

The initial weight ( $W(0)$ ) of each scaffold composition (total  $N = 16$ ) was measured prior to immersing them in a control medium (CM) for varying time durations up to 21 days. The temperature was maintained at 37°C in the presence of 5% CO<sub>2</sub>, and the medium was changed three times a week. Four scaffolds were selected from each composition (total  $N = 4$ ), washed, freeze-dried, and weighed again after 1, 7, 14, and 21 days. All scaffold compositions were evaluated separately. The level of degradation was determined using Equation 2 [73].

$$\text{Degradation degree \% (DD)} = \frac{W(0) - W(f)}{W(0)} \times 100\% \quad (2)$$

### 2.5.4. Accuracy (%):

To evaluate the precision of printing, the consistency between the dimensions of the computer-aided design (CAD) model and the construct was examined. The printing accuracy was determined using Equation 3, where the area of voids ( $n=64$ ) on a single construct was utilized to calculate the printing accuracy percentage (PA). PA was defined as the ratio of the practical and theoretical surface areas ( $A_{\text{void}}$ ) of the voids. The data was collected from four scaffold samples ( $N=4$ ) of each type, and the statistical analysis was averaged. The precision was found to be remarkably high across all printed structures that were created using different ink formulations, demonstrating an accuracy variation of less than 5.5%.

$$\text{Printing accuracy \% (PA)} = \frac{\sum [A_{\text{void}}^{\text{theor}} - \sqrt{(A_{\text{void}}^{\text{pract}} - A_{\text{void}}^{\text{theor}})^2}]}{\sum A_{\text{void}}^{\text{theor}}} \times 100 \quad (3)$$

Where  $A_{\text{void}}^{\text{theor}}$  and  $A_{\text{void}}^{\text{pract}}$  represent the surface areas of theoretical and realistic single voids on a scaffold, respectively.

### 2.5.5. Stress/strain testing:

The texture analyzer (TA-XT2-Stable Micro Systems, U.K) was used to calculate the elastic modulus of the printed scaffolds. To determine the degree of degradation after 1, 7, and 21 days in PBS, compression tests were conducted on the scaffolds. A plunger with a 50mm diameter was employed to compress the samples up to 86% deformation at a speed of 1 mm.s<sup>-1</sup>. The stress-strain curve between 10% and 20% strain was analyzed, and the slope of the linear portion of the curve was calculated using equation (4) to estimate the elastic modulus (E).

$$E = \frac{\frac{F}{A}}{\frac{\Delta h}{h}} \quad (4)$$

In the study, the impact of compression on a scaffold was evaluated by taking measurements using three replicates (N=3) for each trial. The parameters assessed were F (applied force), A (scaffold area),  $\Delta h$  (height change during compression), and h (initial height). The findings presented are the averaged results.

## 2.6 Cell culture:

The NIH/3T3 mouse embryo fibroblast cells, identified as ATCC® CRL-1658™, were grown in a culture medium (CM) comprising DMEM and fetal bovine serum (15%), along with a 1% supplement of penicillin/streptomycin. The cells were kept in a room with 5% CO<sub>2</sub> and maintained at normal temperature. After every 3 days, the cells were detached by trypsin EDTA (0.25%) for passaging.

### 2.6.1. Scaffolds preparation for cell viability:

Following the procedure outlined in [74], fibroblast cells of the NIH/3T3 lineage were seeded onto sterilized, freeze-dried scaffolds and cultured in a CM at 37°C with 5% CO<sub>2</sub>. On days 1, 7, 14, and 21, the viability of the cells in the scaffolds was assessed using live/dead staining. After the culture medium was aspirated, the scaffolds were stained for 40 minutes in an incubator at 37°C with 5% CO<sub>2</sub>, using a staining medium containing 2 M calcein-AM, 4 μM ethidium homodimer, and 5 g/mL Hoechst. The scaffolds were then cleaned (x3) with PBS and transferred into imaging chambers (ibidi, -Slide) filled with CM. Confocal laser scanning microscope LSM 780 (by ZEISS), equipped with an x20 objective and excitation/emission

channels of 404/517 nm for calcein (living), 517/617 nm for ethidium homodimer (dead), and 350/461 nm for Hoechst (nucleus), was used to capture representative images from the scaffold (at a magnification of X20). ImageJ (Fiji) was utilized for cell counting and analysis, and the number of living and dead cells was determined using formula (5) to evaluate cell viability.

$$\text{Cell viability (\%)} = \frac{\#Live}{\#Live + \#dead} \times 100\% \quad (5)$$

For better visualization color enhancement was applied (maximum intensity).

## **2.7. Statistical analysis:**

Origin software was used to evaluate the data. The mean values  $\pm$  standard deviation were used to present quantitative data. ANOVA was employed to compare the data, followed by Tukey's test for pairwise comparisons. Any disparities with a p-value less than 0.05 were regarded as statistically significant.

# CHAPTER 3. RESULTS AND DISCUSSION

## 3.1. FTIR analysis of oxidized Alginate, formulations of bioink and their rheological properties analysis:

Sodium Alginate was oxidized using a sodium periodate. For this, Alginate's vicinal diols can be separated by periodate, producing a dialdehyde derivative in the process. In Figure 3.1, oxidation is clearly demonstrated by the aldehyde band at  $1725\text{ cm}^{-1}$  in the FTIR spectrum.

To create aqueous Gel/OxAlg inks, four ink formulations were developed by combining varying concentrations (3.08%, 2.86%, 2.67%, and 2.50% w/v) of oxidized sodium alginate (OxAlg) with gelatin (Gel) at a 1:1 ratio. Previous research [75] had suggested that these concentrations were ideal for achieving printability and the formation of large pores during cryogenic crosslinking. Gel contributed shear thinning properties to the ink, while OxAlg provided aldehyde groups for chemical crosslinking. The degree of alginate oxidation was set at 10% with  $4\text{ }\mu\text{M}$  glutaraldehyde doping to ensure high porosity and large pore size post-cryogelation and to prevent the rapid degradation of the scaffolds. Rheological testing was used to evaluate the shear-thinning behavior of the four hydrogels, with the 2.50% and 2.67% w/v inks classified as weak gels based on their damping factor ( $\tan \delta$ ) values, which were approximately 0.2 across the temperature range tested. These results are illustrated in Figure 3.2 (A), where the  $\tan \delta$  is plotted against temperature to differentiate between weak and strong gels based on the ratio of loss to storage moduli ( $G''/G'$ ).



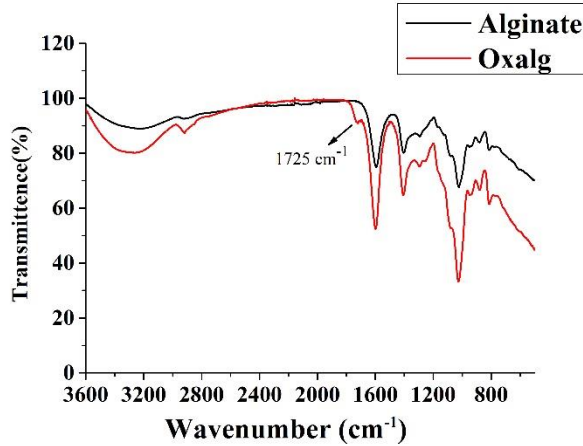


**Figure 3.1** FTIR measurements of alginate(-) and oxidized alginate(-). The oxidation reaction-introduced aldehyde groups' vibrational band is shown by the arrow.

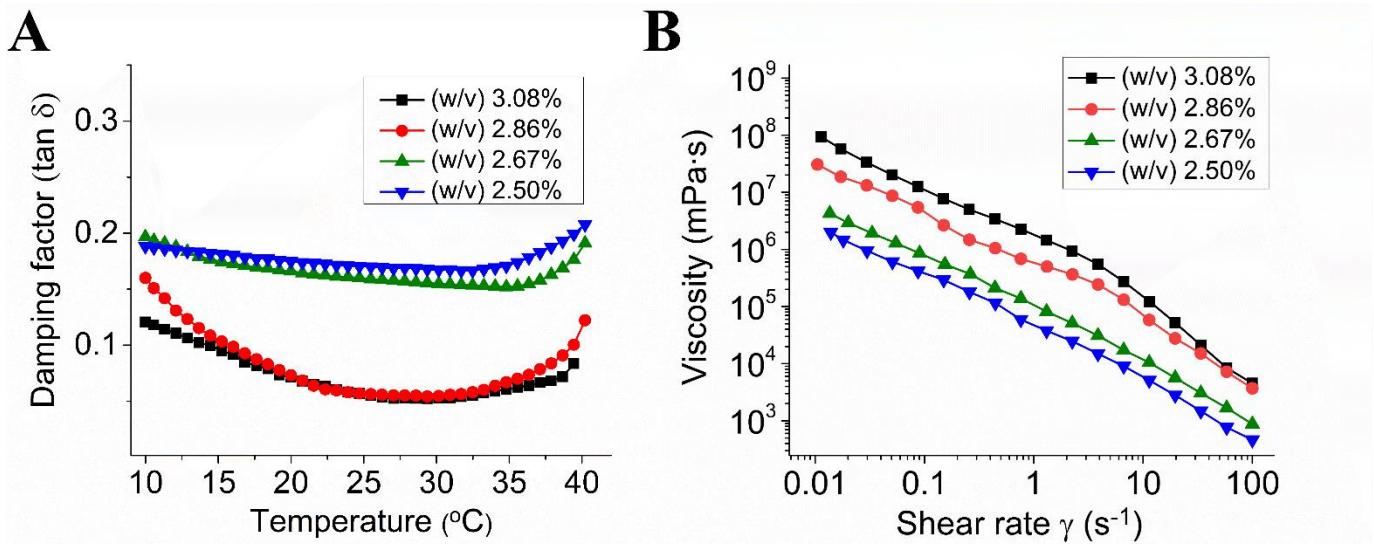


**Figure 3.1** Rheological analysis of gel/OxAlg biopolymer compositions with weight percentages of 3.08%, 2.86%, 2.67%, and 2.50%. (A) damping factor ( $\tan \delta$ ) with temperature, and (B) viscosity versus shear rate.

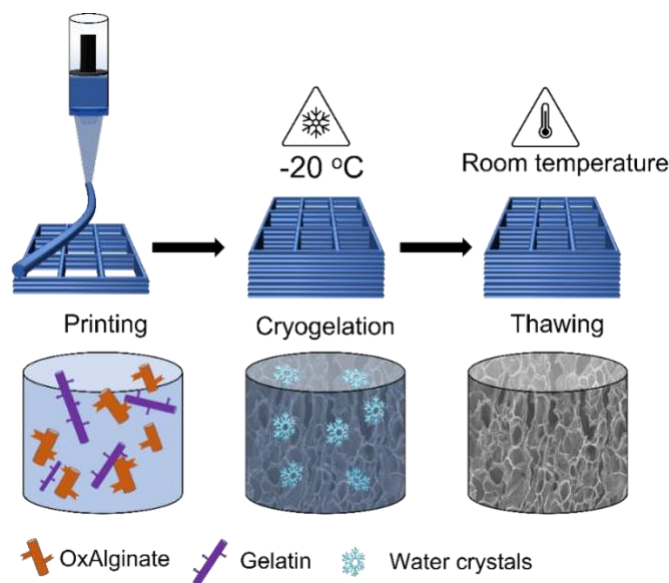
In the study, the hydrogel formulations of 2.86% and 3.08% w/v are represented by the black and red curves, respectively, which exhibit strong gel behavior ( $\tan \delta \leq 0.1$ ). The 3.08% w/v ink demonstrates slightly more stable gel characteristics within the temperature range of  $15 \geq T \geq 10$  oC and  $40 \geq T \geq 35$  oC due to the higher polymer concentration, which predominantly forms hydrogen bonds.

Figure 3.2 (B) displays the non-Newtonian behavior of the inks and their suitability for 3D printing, as

demonstrated by the decreasing trend in viscosity for all ink concentrations as a function of shear rate. The ink's viscosity is found to be directly proportional to the Gel/OxAlg concentration, with the inks ranked based on their viscosity values, indicating varying levels of printing accuracy (PA): 3.08%, 2.86%, 2.67%, and 2.50%.

### 3.2. Printing and characterization of Gelatin/Oxidized Alginate cryogel scaffolds:

Figure 3.3 depicts the process of creating 3D printed hydrogel scaffolds with large pores. To produce four different types of hydrogel scaffolds, a petri dish was used to print 15 layers of square-shaped structures (measuring 12x12x2.85 mm) using inks composed of 1:1 Gel/OxAlg and varying concentrations of 2.50%, 2.67%, 2.86%, and 3.08% w/v.



**Figure 3.3** Cryogelation was used to create macroporous hydrogel scaffolds for 3D printing using Gel/OxAlg. A 3D structure is printed by ink extrusion, followed by 24 hours of cryopolymerization at  $-20\text{ }^{\circ}\text{C}$  and the creation of a macroporous cryogels scaffold after thawing at  $37\text{ }^{\circ}\text{C}$  temperature.

The study produced macroporous hydrogel scaffolds by freezing the structures at  $-20\text{ }^{\circ}\text{C}$  for a day and thawing them at room temperature to create chemically crosslinked structures. Adjustments were made to the printing speed to create 0.45 mm-thick traces during extrusion, as macropores above  $100\text{ }\mu\text{m}$  were formed during the cryo treatment. The mass of the resulting scaffolds of different compositions was found to be less than 5%,

and optical views of the 3D scaffolds made using the four specified (1:1) Gel/OxAlg inks are displayed in Figure 3.4 (A).

To create high-precision scaffolds, the ink's ability to extrude uniform fibers and maintain their structure after deposition is essential. The printing accuracy (PA) was measured to compare the actual scaffold dimensions with the CAD pattern, and the 2.86% w/v composition was found to be the best for 3D printing. Ink with a higher concentration (3.08% w/v) had greater viscosity and stickiness, hindering ink flow and deposition accuracy and reducing the PA to  $33\pm 5.5\%$ .

The scaffolds were created using Gel/OxAlg inks with varying concentrations, frozen at  $-20\text{ }^{\circ}\text{C}$  for 24 hours, and then thawed at room temperature to create chemically crosslinked macroporous hydrogel scaffolds. The macropores were formed during cryo treatment, and printing speed was adjusted accordingly. The mass diversity of the resulting scaffolds of different compositions was less than 5%. The best composition for 3D printing was 2.86% w/v Gel/OxAlg ink, while less concentrated inks, 2.50% and 2.67% w/v, affected the scaffold shape, even at the lowest printing bed temperature of  $4\text{ }^{\circ}\text{C}$ . All the scaffolds had mechanical integrity and comparable pore sizes, but only the scaffolds with 2.86% and 3.08% w/v were able to maintain their preset thickness of 2.85 mm.

Swelling and degradation kinetics of the scaffolds were studied by soaking them in PBS for 1 and 5 hours. The higher concentration scaffolds had an enhanced capacity for swelling, ranging from 1500-2000% of their dry mass after 5 hours, while the lower concentration samples had a significantly lower swelling capacity of only about 400 percentage. The water retention of the scaffolds was consistent over two weeks, with only a slight downward trend for the lower concentration scaffolds. The scaffolds need to be mechanically stable for the first two to three weeks to promote early cell proliferation, and tissue regeneration can take up to eight weeks to complete successfully.

The difference in water uptake between the scaffolds with higher and lower biopolymer concentrations can be attributed to differences in their structural integrity and total accessible pore capacity for water. The lower swelling capacity of the 2.50% and 2.67% w/v scaffolds can be attributed to their disturbed morphology and decreased total pore volume. The degradation test data revealed that the scaffolds with higher biopolymer concentrations, 2.86% and 3.08% w/v, degraded less than the 2.50% and 2.67% w/v scaffolds after three weeks of incubation in PBS at  $37\text{ }^{\circ}\text{C}$ , which can be attributed to differences in their structural integrity, chemical bonding, and degree of crosslinking.

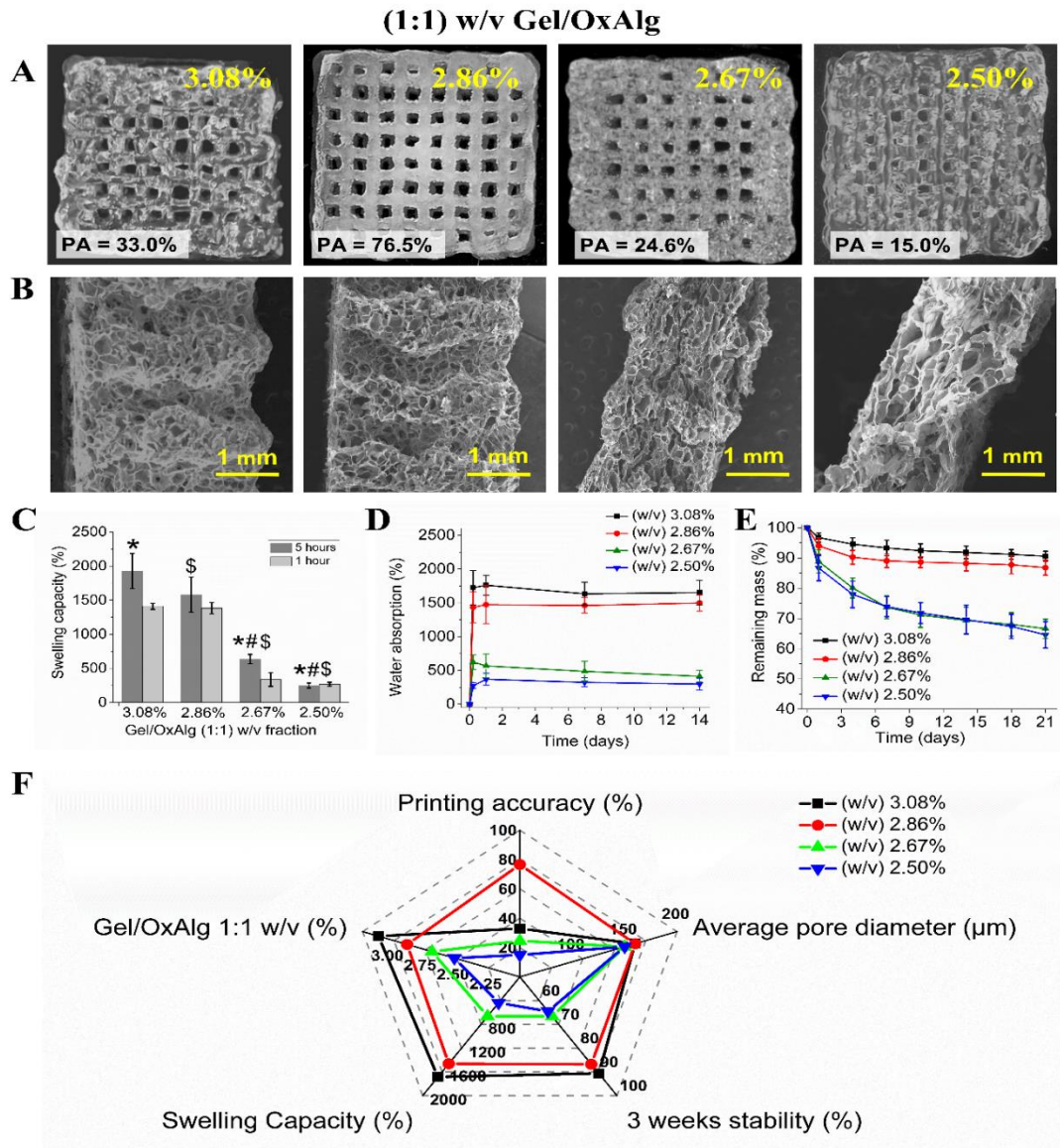


**Figure 3.4** The properties of Gel/OxAlg ink-printed scaffolds with concentrations of 3.08%, 2.86%, 2.67%, and 2.50% (1:1) w/v were analyzed. Optical pictures and SEM cross-sectional view micrographs were taken to show the scaffolds just after printing. The SC of the scaffolds was calculated after one and five hours, as well as their temporal water absorption and degradation rate in PBS at 37 °C (\*#\\$ show significant changes related to the 5 hours measurement with  $p < 0.05$ ). A visual representation in the form of a web chart summarizes the correlation among the ink concentration, PA, and the mechanical and morphological characteristics of the 3D-printed scaffolds, as stated in (F).

*The total number of replicates for all experiments is  $N = 4$ . All investigations utilized a pH value of 7.4.*

The findings suggest that although the 2.67% and 2.50% w/v scaffolds experienced a significant reduction in mass of almost 30% during the two-week degradation test, their ability to absorb water only decreased slightly. This implies that the decline in polymeric content could be due to the degradation of non-porous polymer content and hydrolytic wall weakening, without affecting capillarity.

Figure 3.4(F) demonstrates the features of Gel/OxAlg ink at different concentrations, along with the resulting 3D printed scaffolds' morphological characteristics, temporal stability, and PA. While the printing accuracy is superior for the latter, the mechanical and structural properties of scaffolds created with 2.86% and 3.08% weight percentages are similar. Therefore, we suggest using the 2.86% ink to produce Gel/OxAlg scaffolds with 3D printing technology, and we focus on characterizing it.

### **3.3. Scanning electron microscope and mechanical results of the selected 2.86% w/v Gelatin/Oxidized Alginate scaffold:**

SEM analysis was employed to investigate the configuration and form of the selected scaffold, with a focus on 2.86% w/v. The results of the analysis are displayed in Figures 3.5 (B-D), which showcase the top and cross-sectional view of the scaffold, as well as a magnified view of a representative area. Figure 3.5 (A) illustrates the 15-layer scaffold that was rapidly 3D printed. The SEM micrographs showed the scaffold's mechanical integrity, with a uniformly dispersed and connected microporous network. Additionally, the analysis of the pore size distribution in Figure 3.5 (E) showed that most of the pores' diameter ranged between 160 and 200  $\mu\text{m}$ .

After subjecting the scaffold to deterioration testing for 1, 7, 14, and 21 days, a stress-strain test was performed to demonstrate that the scaffold's physical integrity was maintained for a long time, without compromising its mechanical stability, as illustrated in Figure 3.5 (F). The cryogel exhibited great elasticity, enduring compression, stress, and mass loss even after three weeks in an aqueous solution. Minor variation was observed in the scaffold's elasticity, with the elastic modulus decreasing from 0.12 to 0.09 kPa on 7 days, then restoring to its initial values on day 14 and increasing to  $E = 0.15$  kPa on day 21, after an initial 5% mass degradation caused by uncrosslinked polymer loss on the day 1. The variations in elasticity were attributed to

the weakening of the hydrogel's polymer walls due to degradation, which changed the scaffold's softness, rather than to porosity loss.

Glutaraldehyde doping was used as a second crosslinker to control the printed scaffolds' long-term stability, allowing for stable swelling capacity over time. The absence of glutaraldehyde caused a substantially faster rate of breakdown dynamics than the optimal composition, with total degradation occurring at 10 days. The experimental research showed that a 4  $\mu\text{M}$  concentration of the cross-linking agent had a significant impact on long-term stability without affecting the scaffolds' morphology or the inks' shear thinning properties. Despite visually identical scaffolds after cryogelation, the use of glutaraldehyde ensured greater long-term stability.

(1:1) Gel/OxAlg 2.86% w/v

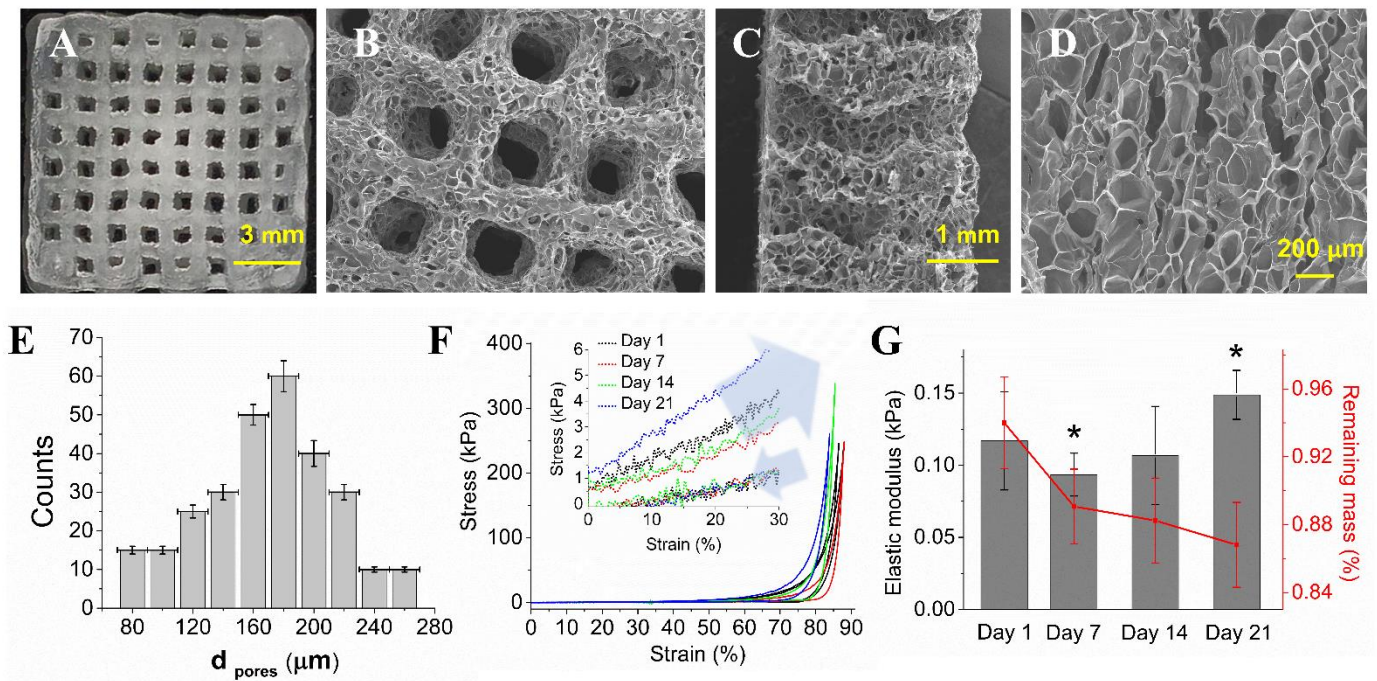


**Figure 3.5** Representation of the 2.86% w/v (1:1) Gel/OxAlg 3D printed scaffold's structural and mechanical properties. The SEM micrographs were taken after cryogelation and included images of the full-size optical print (A), a top view (B), a cross-sectional view (C), and a magnified view of a representative area (D). The histogram data was based on four cubic samples measuring  $2 \times 2 \times 1$  mm in (E) depicts the dispersion of averaged pore diameter. The SEM image was studied using ImageJ's (binary grayscale surface analysis). The elastic moduli were graphed against the scaffold's mass loss after it had been incubated in PBS for durations of 1, 7, 14, and 21 days (F) and stress-strain behavior (Inset: magnified curves at lower strain values) in (G). Significant differences between the sample and other samples are indicated by a (\*) when  $p < 0.05$ .

The stability of scaffolds could potentially be improved through multi-step synthesis involving freezing and thawing cycles to form more covalent bonds. However, it's important to consider potential drawbacks like a longer synthesis process and the possibility of decreasing the average pore size.

### **3.4. Cell seeding efficiency on Gelatin/Oxidized Alginate scaffold (2.86% w/v):**

The successful colonization and seeding of scaffolds by cells are crucial for the formation of the extracellular matrix and integration of the scaffold into the tissue [79,80]. The physical properties of the scaffold can impact cell behavior, and previous studies have indicated that porosity design can enhance long-term cell viability and the establishment of a 3D cellular network within printed scaffolds [81,82].

An investigation was conducted to explore the influence of scaffolds on NIH/3T3 fibroblast cells. The research analyzed changes in cell shape and distribution on porous scaffolds made of Gel/OxAlg 2.86% w/v that were 3D printed over time. Figure 3.6 (A) displays live and dead cell images on days 1, 7, 14, and 21, with green fluorescence indicating that live cells were the predominant population during all periods. After one day, the percentage of viable cells was at least 93%, with a maximum percentage of  $96.1 \pm 4.4\%$ . Figure 3.6 (B) shows that the percentage of viable cells did not differ significantly at various time points. The outcomes suggest that the scaffold maintained normal cell metabolic activity for up to three weeks, and cell seeding was successful. Earlier studies have demonstrated that larger pores in gelatin cryogels resulted in lower cell densities due to cell escape through the pores, resulting in decreased seeding efficiency [83,84].

Cell morphology affects the integration of biomaterials, and having a healthy cell morphology often indicates good cell adhesion, resulting in proper cell function and biocompatibility [85]. Figure 3.6 (A) displays a combination of images taken on days 1, 7, 14, and 21, demonstrating various cell morphologies in the printed scaffolds over time. The images show an overlay of live/dead staining with nucleus staining, providing information about the morphology of the cells within the printed scaffolds. The magnified regions in the right column show individual cells in detail. The cells in the scaffolds were predominantly spherical, with little cytoplasm visible in the images, and few elongated cells after the first day. The cell morphology became elongated on days 7 and 14, but by day 21, most of the cells were dispersed and formed a network of interconnected cells. After three weeks of observation, it was determined that the 2.86% w/v scaffolds were safe and suitable for various biomedical and tissue engineering applications.

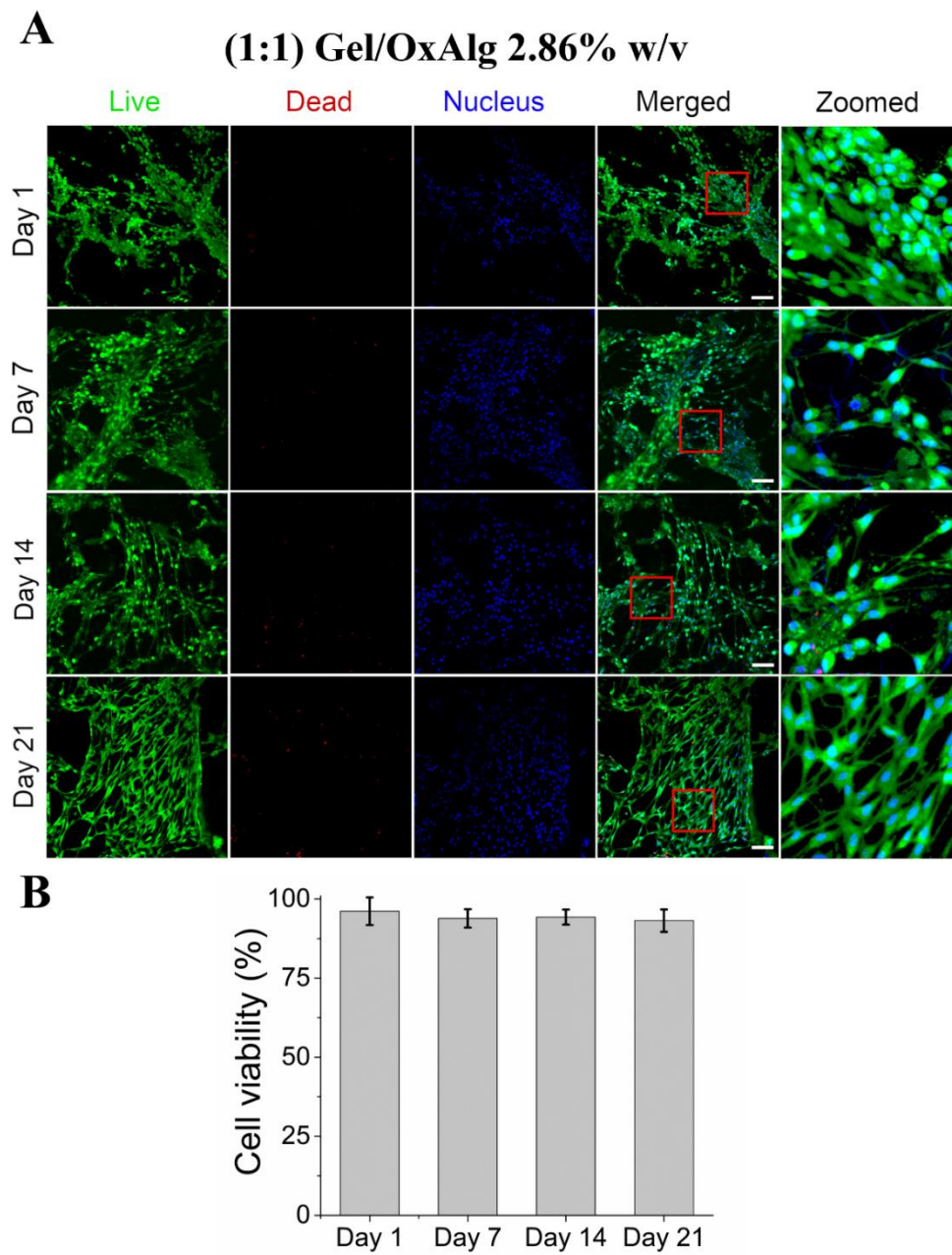


**Figure 3.6** Using NIH/3T3 fibroblast cells, 3D printed 2.86% Gel/OxAlg cryogels were characterized in vitro. (A) Illustrations of the cryogels following cell seeding at days 1, 7, 14, and 21 using live/dead staining. The color green denotes fluorescence in living cells, while red represents fluorescence in dead cells. Cell nuclei are seen as blue (Hoechst 33342). The combined column of images displays live/dead staining with Hoechst overlaid. Individual stained cells are seen in zoomed images from the specified locations. With the program Zen light, color enhancement was made for improved visibility (maximum intensity). 100  $\mu$ m is shown by the scale bar. (B) Quantitative study of the cell viability on days 1, 7, 14, and 21.



# CHAPTER 4. CONCLUSION

The Gel/OxAlg mixes with a low concentration of 1:1 can be utilized as inks to generate hydrogel scaffolds for 3D printing. By merging single-step cryogenic synthesis and 3D printing technology, it is feasible to create low-cost scaffolds with high accuracy and pore morphology of super-hundred-microns. Nonetheless, as cryo synthesis necessitates exposure to extremely cold temperatures, producing cell-filled scaffolds in a single step, as recommended by bioprinting, is not achievable. Nevertheless, the scaffolds that are generated display a distinctive shape and biocompatibility, making them promising for various tissue regeneration purposes.

Scaffolds with a PA higher than 75% can be effectively produced through 3D printing using a blend of Gel/OxAlg at a concentration of 2.86% w/v (1:1). These scaffolds have exceptional swelling ability and can expand up to 1800% of their initial dry weight, which supports cell migration. Additionally, they provide sufficient mechanical support for temporary usage and tissue volume preservation. The scaffolds maintained over 85% of their initial mass and had good elasticity, with a value of about 0.15 kPa, after being exposed to aqueous conditions for three weeks. The 2.86% w/v (1:1) Gel/OxAlg scaffold has highly attractive structural features, long-lasting mechanical stability and integrity, good biocompatibility, and a unique extra-large porous morphology, making it ideal for use in tissue engineering applications.

# REFERENCES

- [1] Zhou J, Zhang Z, Joseph J, Zhang X, Ferdows BE, Patel DN, Chen W, Banfi G, Molinaro R, Cosco D, Kong N. Biomaterials and nanomedicine for bone regeneration: Progress and future prospects. *InExploration* 2021 Oct (Vol. 1, No. 2, p. 20210011).
- [2] Alkhursani SA, Ghobashy MM, Al-Gahtany SA, Meganid AS, Abd El-Halim SM, Ahmad Z, Khan FS, Atia GA, Cavalu S. Application of Nano-Inspired Scaffolds-Based Biopolymer Hydrogel for Bone and Periodontal Tissue Regeneration. *Polymers*. 2022 Sep 10;14(18):3791.
- [3] Ansari M. Bone tissue regeneration: biology, strategies and interface studies. *Progress in biomaterials*. 2019 Dec;8(4):223-37.
- [4] Von Euw S, Wang Y, Laurent G, Drouet C, Babonneau F, Nassif N, Azais T. Bone mineral: new insights into its chemical composition. *Scientific reports*. 2019 Jun 11;9(1):1-1.
- [5] Emmons AL, Mundorff AZ, Keenan SW, Davoren J, Andronowski J, Carter DO, DeBruyn JM. Characterizing the postmortem human bone microbiome from surface-decomposed remains. *PLoS one*. 2020 Jul 8;15(7):e0218636.
- [6] Hayashi K, Kishida R, Tsuchiya A, Ishikawa K. Carbonate apatite micro-honeycombed blocks generate bone marrow-like tissues as well as bone. *Advanced Biosystems*. 2019 Dec;3(12):1900140.
- [7] Zhang X, Koo S, Kim JH, Huang X, Kong N, Zhang L, Zhou J, Xue J, Harris MB, Tao W, Kim JS. Nanoscale materials-based platforms for the treatment of bone-related diseases. *Matter*. 2021 Sep 1;4(9):2727-64.
- [8] Malliappan SP, Yetisgin AA, Sahin SB, Demir E, Cetinel S. Bone tissue engineering: Anionic polysaccharides as promising scaffolds. *Carbohydrate polymers*. 2022 Jan 18;119:142.
- [9] Chen Z, Zhang W, Wang M, Backman LJ, Chen J. Effects of Zinc, Magnesium, and Iron Ions on Bone Tissue Engineering. *ACS Biomaterials Science & Engineering*. 2022 May 31.
- [10] Ott SM. Cortical or trabecular bone: what's the difference?. *American journal of nephrology*. 2018 Jul 1;47(6):373-6.
- [11] Pan CY, Liu PH, Tseng YC, Chou ST, Wu CY, Chang HP. Effects of cortical bone thickness and trabecular bone density on primary stability of orthodontic mini-implants. *Journal of dental sciences*. 2019 Dec 1;14(4):383-8.
- [12] Kaur M. Titanium-based view on titanium and titanium orthopedics as biomaterials for

- orthopaedic applications. *Materials Science and Engineering: C*. 2019 Sep 1;102:844-62.
- [13] Morgan EF, Unnikrisnan GU, Hussein AI. Bone mechanical properties in healthy and diseased states. *Annual review of biomedical engineering*. 2018 Jun 6;20:119.
- [14] Qu H, Fu H, Han Z, Sun Y. Biomaterials for bone tissue engineering scaffolds: A review. *RSC advances*. 2019;9(45):26252-62.
- [15] Perez JR, Kouroupis D, Li DJ, Best TM, Kaplan L, Correa D. Tissue engineering and cell-based therapies for fractures and bone defects. *Frontiers in bioengineering and biotechnology*. 2018 Jul 31;6:105.
- [16] Nayak S, Manivasagam G, Sen D. Progress of regenerative therapy in orthopedics. *Current Osteoporosis Reports*. 2018 Apr;16(2):169-81.
- [17] Liu F, Zhang DZ, Zhang P, Zhao M, Jafar S. Mechanical properties of optimized diamond lattice structure for bone scaffolds fabricated via selective laser melting. *Materials*. 2018 Mar 3;11(3):374.
- [18] Egan PF. Integrated design approaches for 3D printed tissue scaffolds: Review and outlook. *Materials*. 2019 Jul 24;12(15):2355.
- [19] Roseti L, Parisi V, Petretta M, Cavallo C, Desando G, Bartolotti I, Grigolo B. Scaffolds for bone tissue engineering: state of the art and new perspectives. *Materials Science and Engineering: C*. 2017 Sep 1;78:1246-62.
- [20] Collins MN, Ren G, Young K, Pina S, Reis RL, Oliveira JM. Scaffold fabrication technologies and structure/function properties in bone tissue engineering. *Advanced Functional Materials*. 2021 May;31(21):2010609.
- [21] Pishavar E, Luo H, Naserifar M, Hashemi M, Toosi S, Atala A, Ramakrishna S, Behravan J. Advanced hydrogels as exosome delivery systems for osteogenic differentiation of MSCs: application in bone regeneration. *International Journal of Molecular Sciences*. 2021 Jun 8;22(12):6203.
- [22] Diba M, Koons GL, Bedell ML, Mikos AG. 3D printed colloidal biomaterials based on photo-reactive gelatin nanoparticles. *Biomaterials*. 2021 Jul 1;274:120871.
- [23] Adel IM, ElMeligy MF, Elkasabgy NA. Conventional and recent trends of scaffolds fabrication: a superior mode for tissue engineering. *Pharmaceutics*. 2022 Jan 27;14(2):306.
- [24] Pedrero SG, Llamas-Sillero P, Serrano-López J. A multidisciplinary journey towards bone tissue engineering. *Materials*. 2021 Aug 28;14(17):4896.

- [25] Melke J, Midha S, Ghosh S, Ito K, Hofmann S. Silk fibroin as biomaterial for bone tissue engineering. *Acta biomaterialia*. 2016 Feb 1;31:1-6.
- [26] Venkatesan J, Bhatnagar I, Manivasagan P, Kang KH, Kim SK. Alginate composites for bone tissue engineering: A review. *International journal of biological macromolecules*. 2015 Jan 1;72:269-81.
- [27] Wright B, De Bank PA, Luetchford KA, Acosta FR, Connon CJ. Oxidized alginate hydrogels as niche environments for corneal epithelial cells. *Journal of Biomedical Materials Research Part A*. 2014 Oct;102(10):3393-400.
- [28] Hernández-González AC, Téllez-Jurado L, Rodríguez-Lorenzo LM. Alginate hydrogels for bone tissue engineering, from injectables to bioprinting: A review. *Carbohydrate polymers*. 2020 Feb 1;229:115514.
- [29] Celikkin N, Mastrogiacomo S, Jaroszewicz J, Walboomers XF, Swieszkowski W. Gelatin methacrylate scaffold for bone tissue engineering: the influence of polymer concentration. *Journal of Biomedical Materials Research Part A*. 2018 Jan;106(1):201-9.
- [30] Singh G, Singh RP, Jolly SS. Customized hydroxyapatites for bone-tissue engineering and drug delivery applications: A review. *Journal of Sol-Gel Science and Technology*. 2020 Jun;94(3):505-30.
- [31] Chan KH, Zhuo S, Ni M. Natural and synthetic peptide-based biomaterials for bone tissue engineering. *OA Tiss Eng*. 2013;1(1):6.
- [32] Hulbert SF, Morrison SJ, Klawitter JJ. Compatibility of porous ceramics with soft tissue; application to tracheal prostheses. *Journal of Biomedical Materials Research*. 1971 Nov;5(6):269-79.
- [33] Sood A, Ji SM, Kumar A, Han SS. Enzyme-Triggered Crosslinked Hybrid Hydrogels for Bone Tissue Engineering. *Materials*. 2022 Sep 14;15(18):6383.
- [34] Gu L, Shan T, Ma YX, Tay FR, Niu L. Novel biomedical applications of crosslinked collagen. *Trends in biotechnology*. 2019 May 1;37(5):464-91.
- [35] Zhai P, Peng X, Li B, Liu Y, Sun H, Li X. The application of hyaluronic acid in bone regeneration. *International journal of biological macromolecules*. 2020 May 15;151:1224-39.
- [36] Nezhad-Mokhtari P, Ghorbani M, Roshangar L, Rad JS. Chemical gelling of hydrogels-based biological macromolecules for tissue engineering: Photo-and enzymatic-crosslinking methods. *International journal of biological macromolecules*. 2019 Oct 15;139:760-72.

- [37] Oryan A, Kamali A, Moshiri A, Baharvand H, Daemi H. Chemical crosslinking of biopolymeric scaffolds: Current knowledge and future directions of crosslinked engineered bone scaffolds. *International journal of biological macromolecules*. 2018 Feb 1;107:678-88.
- [38] Taherkhani S, Moztarzadeh F. Fabrication of a poly ( $\epsilon$ -caprolactone)/starch nanocomposite scaffold with a solvent-casting/salt-leaching technique for bone tissue engineering applications. *Journal of Applied Polymer Science*. 2016 Jun 15;133(23).
- [39] Zopf DA, Flanagan CL, Mitsak AG, Brennan JR, Hollister SJ. Pore architecture effects on chondrogenic potential of patient-specific 3-dimensionally printed porous tissue bioscaffolds for auricular tissue engineering. *International journal of pediatric otorhinolaryngology*. 2018 Nov 1;114:170-4.
- [40] Ke D, Bose S. Effects of pore distribution and chemistry on physical, mechanical, and biological properties of tricalcium phosphate scaffolds by binder-jet 3D printing. *Additive Manufacturing*. 2018 Aug 1;22:111-7.
- [41] Pan S, Zhong Y, Shan Y, Liu X, Xiao Y, Shi H. Selection of the optimum 3D-printed pore and the surface modification techniques for tissue engineering tracheal scaffold in vivo reconstruction. *Journal of Biomedical Materials Research Part A*. 2019 Feb;107(2):360-70.
- [42] Kelly CN, Miller AT, Hollister SJ, Guldborg RE, Gall K. Design and structure–function characterization of 3D printed synthetic porous biomaterials for tissue engineering. *Advanced healthcare materials*. 2018 Apr;7(7):1701095.
- [43] Rabionet M, Guerra AJ, Puig T, Ciurana J. 3D-printed tubular scaffolds for vascular tissue engineering. *Procedia Cirp*. 2018 Jan 1;68:352-7.
- [44] Diaz-Gomez L, Kontoyiannis PD, Melchiorri AJ, Mikos AG. Three-dimensional printing of tissue engineering scaffolds with horizontal pore and composition gradients. *Tissue Engineering Part C: Methods*. 2019 Jul 1;25(7):411-20.
- [45] Deng F, Liu L, Li Z, Liu J. 3D printed Ti6Al4V bone scaffolds with different pore structure effects on bone ingrowth. *Journal of Biological Engineering*. 2021 Dec;15(1):1-3.
- [46] Brauker JH, Carr-Brendel VE, Martinson LA, Crudele J, Johnston WD, Johnson RC. Neovascularization of synthetic membranes directed by membrane microarchitecture. *Journal of biomedical materials research*. 1995 Dec;29(12):1517-24.
- [47] Wang W, Caetano G, Ambler WS, Blaker JJ, Frade MA, Mandal P, Diver C, Bártolo P. Enhancing the hydrophilicity and cell attachment of 3D printed PCL/graphene scaffolds for bone

tissue engineering. *Materials*. 2016 Dec 7;9(12):992.

[48] Wu S, Liu X, Yeung KW, Liu C, Yang X. Biomimetic porous scaffolds for bone tissue engineering. *Materials Science and Engineering: R: Reports*. 2014 Jun 1;80:1-36.

[49] Motamedian SR, Hosseinpour S, Ahsaie MG, Khojasteh A. Smart scaffolds in bone tissue engineering: A systematic review of literature. *World journal of stem cells*. 2015 Apr 26;7(3):657.

[50] Rodriguez-Enriquez S, Kim I, Currin RT, Lemasters JJ. Tracker dyes to probe mitochondrial autophagy (mitophagy) in rat hepatocytes. *Autophagy*. 2006 Jan 9;2(1):39-46.

[51] Mohd Hilmi AB, Halim AS, Hassan A, Lim CK, Noorsal K, Zainol I. In vitro characterization of a chitosan skin regenerating template as a scaffold for cells cultivation. *Springerplus*. 2013 Dec;2(1):1-9.

[52] Wartenberg A, Weisser J, Schnabelrauch M. Glycosaminoglycan-Based Cryogels as Scaffolds for Cell Cultivation and Tissue Regeneration. *Molecules*. 2021 Jan;26(18):5597.

[53] Kudaibergen G, Zhunussova M, Mun EA, Arinova A, Ogay V. Studying the Effect of Chondroitin Sulfate on the Physicochemical Properties of Novel Gelatin/Chitosan Biopolymer-Based Cryogels. *Applied Sciences*. 2021 Jan;11(21):10056.

[54] Şarkaya K, Akıncioğlu G, Akıncioğlu S. Investigation of tribological properties of HEMA-based cryogels as potential articular cartilage biomaterials. *Polymer-Plastics Technology and Materials*. 2022 Mar 7:1-7.

[55] Hu T, Shi M, Zhao X, Liang Y, Bi L, Zhang Z, Liu S, Chen B, Duan X, Guo B. Biomimetic 3D aligned conductive tubular cryogel scaffolds with mechanical anisotropy for 3D cell alignment, differentiation and in vivo skeletal muscle regeneration. *Chemical Engineering Journal*. 2022 Jan 15;428:131017.

[56] Carlström IE, Rashad A, Campodoni E, Sandri M, Syverud K, Bolstad AI, Mustafa K. Cross-linked gelatin-nanocellulose scaffolds for bone tissue engineering. *Materials Letters*. 2020 Apr 1;264:127326.

[57] Janoušková O. Synthetic polymer scaffolds for soft tissue engineering. *Physiological research*. 2018 Aug 2;67.

[58] He T, Li B, Colombani T, Joshi-Navare K, Mehta S, Kisiday J, Bencherif SA, Bajpayee AG. Hyaluronic acid-based shape-memory cryogel scaffolds for focal cartilage defect repair. *Tissue Engineering Part A*. 2021 Jun 1;27(11-12):748-60.

- [59] Chen TC, Wong CW, Hsu SH. Three-dimensional printing of chitosan cryogel as injectable and shape recoverable scaffolds. *Carbohydrate Polymers*. 2022 Jun 1;285:119228.
- [60] Pacelli S, Di Muzio L, Paolicelli P, Fortunati V, Petralito S, Trilli J, Casadei MA. Dextran-polyethylene glycol cryogels as spongy scaffolds for drug delivery. *International Journal of Biological Macromolecules*. 2021 Jan 1;166:1292-300.
- [61] Khan MU, Al-Thebaiti MA, Hashmi MU, Aftab S, Abd Razak SI, Abu Hassan S, Abdul Kadir MR, Amin R. Synthesis of silver-coated bioactive nanocomposite scaffolds based on grafted beta-glucan/hydroxyapatite via freeze-drying method: Anti-microbial and biocompatibility evaluation for bone tissue engineering. *Materials*. 2020 Feb 21;13(4):971.
- [62] Li Y, Zhu J, Cheng H, Li G, Cho H, Jiang M, Gao Q, Zhang X. Developments of advanced electrospinning techniques: A critical review. *Advanced Materials Technologies*. 2021 Nov;6(11):2100410.
- [63] Jammalamadaka U, Tappa K. Recent advances in biomaterials for 3D printing and tissue engineering. *Journal of functional biomaterials*. 2018 Mar 1;9(1):22.
- [64] Zhu W, Ma X, Gou M, Mei D, Zhang K, Chen S. 3D printing of functional biomaterials for tissue engineering. *Current opinion in biotechnology*. 2016 Aug 1;40:103-12.
- [65] Bhatt A, Anbarasu A. Nanoscale Biomaterials for 3D printing. *IOSR J Pharm Biol Sci*. 2017;12:80-6.
- [66] Moroni L, Burdick JA, Highley C, Lee SJ, Morimoto Y, Takeuchi S, Yoo JJ. Biofabrication strategies for 3D in vitro models and regenerative medicine. *Nature Reviews Materials*. 2018 May;3(5):21-37.
- [67] Zhang S, Vijayavenkataraman S, Lu WF, Fuh JY. A review on the use of computational methods to characterize, design, and optimize tissue engineering scaffolds, with a potential in 3D printing fabrication. *Journal of Biomedical Materials Research Part B: Applied Biomaterials*. 2019 Jul;107(5):1329-51.
- [68] Wang C, Huang W, Zhou Y, He L, He Z, Chen Z, He X, Tian S, Liao J, Lu B, Wei Y. 3D printing of bone tissue engineering scaffolds. *Bioactive materials*. 2020 Mar 1;5(1):82-91.
- [69] Chowdhury SR, Lokanathan Y, Xian LJ, Busra FM, Yazid MD, Sulaiman N, Lahiry G, Hoque ME. 3D Printed Bioscaffolds for Developing Tissue-Engineered Constructs. In *Design and Manufacturing 2020* May 28. IntechOpen.
- [70] Habib A, Sathish V, Mallik S, Khoda B. 3D printability of alginate-carboxymethyl cellulose

hydrogel. *Materials*. 2018 Mar 20;11(3):454.

[71] D. Berillo, N. Volkova, Preparation and physicochemical characteristics of cryogel based on gelatin and oxidised dextran, *J. Mater. Sci.* 49 (2014) 4855–4868.

[72] C. Tang, L. Yin, J. Yu, C. Yin, Y. Pei, Swelling behavior and biocompatibility of carbopol-containing superporous hydrogel composites, *J. Appl. Polym. Sci.* 104 (2007) 2785–2791.

[73] Pan, W. Song, X. Cao, Y. Wang, 3D Bioplotting of Gelatin/Alginate Scaffolds for Tissue Engineering: Influence of Crosslinking Degree and Pore Architecture on Physicochemical Properties, *J. Mater. Sci. Technol.* 32 (2016) 889–900.

[74] J.T.Y. Lee, K.L. Chow, SEM sample preparation for cells on 3D scaffolds by freeze-drying and HMDS, *Scanning*. 34 (2012) 12–25.

[75] D. Akilbekova, M. Shaimerdenova, S. Adilov, D. Berillo, Biocompatible scaffolds based on natural polymers for regenerative medicine, *Int. J. Biol. Macromol.* 114 (2018) 324–333.

[76] N. Volkova, D. Berillo, Water Uptake as a Crucial Factor on the Properties of Cryogels of Gelatine Cross-Linked by Dextran Dialdehyde, *Gels* 2021, Vol. 7, Page 159. 7 (2021) 159.

[77] H.J. Lee, S.H. Ahn, G.H. Kim, Three-dimensional collagen/alginate hybrid scaffolds functionalized with a drug delivery system (DDS) for bone tissue regeneration, *Chem. Mater.* 24 (2012) 881–891.

[78] A. Subramanian, U.M. Krishnan, S. Sethuraman, Development of biomaterial scaffold for nerve tissue engineering: Biomaterial mediated neural regeneration., *J. Biomed. Sci.* 16 (2009) 108.

[79] D.J. Borg, P.B. Welzel, M. Grimmer, J. Friedrichs, M. Weigelt, C. Wilhelm, M. Prewitz, A. Stißel, A. Hommel, T. Kurth, U. Freudenberg, E. Bonifacio, C. Werner, Macroporous biohybrid cryogels for co-housing pancreatic islets with mesenchymal stromal cells, *Acta Biomater.* 44 (2016) 178–187.

[80] F.S.L. Bobbert, A.A. Zadpoor, Effects of bone substitute architecture and surface properties on cell response, angiogenesis, and structure of new bone, *J. Mater. Chem. B.* 5 (2017) 6175–6192.

[81] A.J. Engler, S. Sen, H.L. Sweeney, D.E. Discher, Matrix Elasticity Directs Stem Cell Lineage Specification, *Cell*. 126 (2006) 677–689.

[82] J. Zhang, E. Wehrle, J.R. Vetsch, G.R. Paul, M. Rubert, R. Müller, Alginate dependent changes of physical properties in 3D bioprinted cell-laden porous scaffolds affect cell viability



and cell morphology, *Biomed. Mater.* 14 (2019).

[83] D. Akilbekova, M. Shaimerdenova, S. Adilov, D. Berillo, Biocompatible scaffolds based on natural polymers for regenerative medicine, *Int. J. Biol. Macromol.* 114 (2018).

[84] N. Ghavidel Mehr, X. Li, M.B. Ariganello, C.D. Hoemann, B.D. Favis, Poly( $\epsilon$ -caprolactone) scaffolds of highly controlled porosity and interconnectivity derived from co-continuous polymer blends: model bead and cell infiltration behavior, *J. Mater. Sci. Mater. Med.* 25 (2014) 2083–2093.

[85] H.C. Bygd, D. Akilbekova, A. Muñoz, K.D. Forsmark, K.M. Bratlie, Poly-l-arginine based materials as instructive substrates for fibroblast synthesis of collagen, *Biomaterials.* 63 (2015).